REPORT DOCUMENTATION PAGE

Form Approved
OMB No. 0704-0188

1. AGENCY USE ONLY (Leave blank)	2. REPORT DATE	3. REPORT TYPE AND DATES COVERED
	2/16/96	Final Technical 03/01/93 to 08/31/95

4. TITLE AND SUBTITLE
Comprehensive Investigation of Low- and High- Power Arcjet Operation

5. FUNDING NUMBERS
Contract No.
F49620-93-1-0213
2308/AS

6. AUTHOR(S)
Erwin, Daniel

7. PERFORMING ORGANIZATION NAME(S) AND ADDRESS(ES)
University of Southern California
Department of Aerospace Engineering
854 W. 36th Place
Los Angeles, CA 90089-1191

8. PERFORMING ORGANIZATION REPORT NUMBER
AFOSR-TR-96
0111

9. SPONSORING/MONITORING AGENCY NAME(S) AND ADDRESS(ES)
Mitat Birkan
AFOSR/NA
110 Duncan Avenue, Suite B115
Bolling AFB, DC 20332-0001

11. SUPPLEMENTARY NOTES

12a. DISTRIBUTION/AVAILABILITY STATEMENT
Approved for public release: Distribution unlimited

12b. DISTRIBUTION CODE

13. ABSTRACT (Maximum 200 words)

Experimental investigation of several aspects of arcjet operation is performed using several diagnostic techniques developed here. Two techniques address the outstanding experimental problem of measurement of plume species density. These are pulsed-electron-beam fluorescence and two-photon laser-induced fluorescence. The former provides data on both molecular and atomic properties, while the latter measures only ground-state atom properties. Ground-state atomic hydrogen density is meaured here for the first time. Current-modulation velocimetry is applied to the study of plume velocity fluctuations. It is found that they exhibit no correlation with the supply current ripple and thus seem to be random.

14. SUBJECT TERMS	15. NUMBER OF PAGES
Arcjet, pulsed-electron-beam fluorescence, arcjet diagnostics, pulsed-electron gun	38
	16. PRICE CODE

17. SECURITY CLASSIFICATION OF REPORT	18. SECURITY CLASSIFICATION OF THIS PAGE	19. SECURITY CLASSIFICATION OF ABSTRACT	20. LIMITATION OF ABSTRACT
Unclassified	Unclassified	Unclassified	UL

FINAL TECHNICAL REPORT:
Comprehensive Investigation of Low- and High-Power Arcjet Operation
3/1/93–8/31/95

Daniel A. Erwin
University of Southern California
Department of Aerospace Engineering
Los Angeles, California 90089-1191
(213) 740-5358; fax (213) 740-7774

Air Force Office of Scientific Research
F49620-93-1-0213

Abstract

Experimental investigation of several aspects of arcjet operation is performed using several diagnostic techniques developed here. Two techniques address the outstanding experimental problem of measurement of plume species density. These are pulsed-electron-beam fluorescence and two-photon laser-induced fluorescence. The former provides data on both molecular and atomic properties, while the latter measures only ground-state atom properties. Ground-state atomic hydrogen density is measured here for the first time. Current-modulation velocimetry is applied to the study of plume velocity fluctuations. It is found that they exhibit no correlation with the supply current ripple and thus seem to be random.

Contents

1. Introduction

Arcjets are expected to play an ever increasing role in satellite propulsion needs, primarily for stationkeeping and on-orbit maneuvering in the near term. While the technology is considered viable enough to be deployed on a Telstar IV communications satellite for stationkeeping,[1.1] arcjet technology is far from maturity. In order to compete successfully with chemical propulsion systems for on-orbit missions, further improvements in arcjet propulsion systems are still required.[1.2] If needed improvements in the performance level and efficiency of arcjets are to be achieved, an increased understanding of the fundamental physical processes that govern the operation of an arcjet is essential. In addition, an ability to predict the plume behavior of a space propulsion device is necessary for prediction and amelioration of damaging plume-spacecraft interactions.

Significant arcjet energy loss results from velocity profile losses due to thick internal boundary layers in the arcjet nozzle and from frozen flow losses such as molecular dissociation. To quantify profile losses, both gas velocity and density distributions must be known. In addition, arcjet models, which are necessary for timely and cost-effective improvements to design, must be tested by comparison with key physical parameters.

For measuring excited state atomic hydrogen velocity and temperature, excited state laser-induced fluorescence[1.3,1.4] has proven to be accurate and essentially non-intrusive. Though the excited states of hydrogen are more easily accessible, most atoms in the plume region are expected to be in the ground state. The ability to measure ground state atomic hydrogen temperature and velocity in addition to density would allow examination of any differences in temperature and velocity between the excited state and ground state species in the non-equilibrium arcjet plume environment.

More importantly, computational calculation of thruster efficiency is based on momentum flux, so that exhaust density as well as velocity must be known.

At present, only limited inroads have been made into the problem of plume density measurements. For hydrogen arcjet thrusters, determination of species density has previously only been accomplished through the use of absorption spectroscopy techniques.[1.5,1.6] These VUV and XUV spectroscopy approaches are quite difficult to implement in practice and are limited to determination of line-of-sight averaged number densities at downstream locations in the plume where the optical depth is not high. These techniques have not been applicable in the determination of atomic density profiles at the thruster nozzle exit, data that is desired in order to calibrate and verify recent advanced computational arcjet modeling results.[1.7–1.12]

The density of atoms relative to the density of molecules in the arcjet thruster is an indication of how much energy is lost into dissociation of the hydrogen molecules and not recovered through recombination into translational kinetic modes. To determine the molecular dissociation fraction and the significance of this energy loss mechanism, the molecular species density needs to be known as well as the atomic number density. The

recent use of Raman spectroscopy[1.13,1.14] in an arcjet plume has provided the first information on molecular hydrogen densities at the arcjet nozzle plane.

It has become obvious that there is a need for determination of atomic ground state hydrogen densities at the nozzle exit of the hydrogen arcjet to support ongoing modeling efforts and to quantify the significance of frozen flow losses such as molecular dissociation.

In this work, two approaches are taken to density measurement. These are pulsed electron-beam fluorescence and two-photon laser-induced fluorescence.

Several of the computational approaches to arcjet simulation are in principle time-accurate. Therefore, they may be used to investigate instability or fluctuations in arcjet operation (arc length fluctuation, rotation of anode attachment spot, etc.). These time-dependent phenomena may be inherent to arcjet operation or may be caused by interaction with the power-processing unit. However, experimental diagnostic techniques such as laser-induced fluorescence perform time-averaging and thus give results averaged over any fluctuations.

To address this, the present work has developed a time-resolved technique, current-modulation velocimetry, which has demonstrated significant fluctuations in arcjet plume velocity.

2. Work Performed

2.1 High-throughput test facility at USC

One objective of this work was to develop the ability at USC to perform testing of kilowatt-class arcjets under realistic, i.e., low-back-pressure chamber conditions. At the outset, our chamber was pumped by a Roots-Stokes combination of about 450 cfm. This led to 1-kW arcjet operation at chamber pressure of order 2 torr. This was clearly unacceptable for investigation of either thrust or plume behavior, because the exhaust was overexpanded; indeed, under some conditions, shock diamonds were visible in the plume.

It was our goal to be able to operate 1-kW arcjets with chamber pressure below 100 millitorr. We therefore deemed it necessary to refit the chamber with a much higher-capacity pumping plant. However, the optical access to the chamber was also considered critical. Prior to the refit, the chamber's optical access was excellent, with large ports on both sides, a smaller top port, and an end window for axial access; this was accomplished via a ninety-degree bend in the six-inch glass pump line. Electrical and gas feedthroughs came through a top flange.

Under this contract, the chamber was refitted with a three-stage Roots-Roots-Stokes pumping combination, which operates at 6500 cfm. See figure 2.1. The pump line is an eight-foot straight run of 12-inch pipe. An air-operated gate valve allows the chamber to be used statically, and assists with vacuum diagnostics of the pumping system. A rubber bellows at the pump end of the pump line, and a steel bellows on the chamber end, provide vibration isolation.

The asymmetric pumping configuration (with non-axial gas flow) was chosen in order to maximize optical access as well as pump line throughput.

After refit, the facility operates very well. At full power on a 1-kW hydrogen arcjet, the chamber pressure is 65 millitorr, well under the design specification. Vibration isolation is good enough to use the Aerospace Corporation thrust stand (based on the NASA Lewis ion-engine thrust stand design) without difficulty.

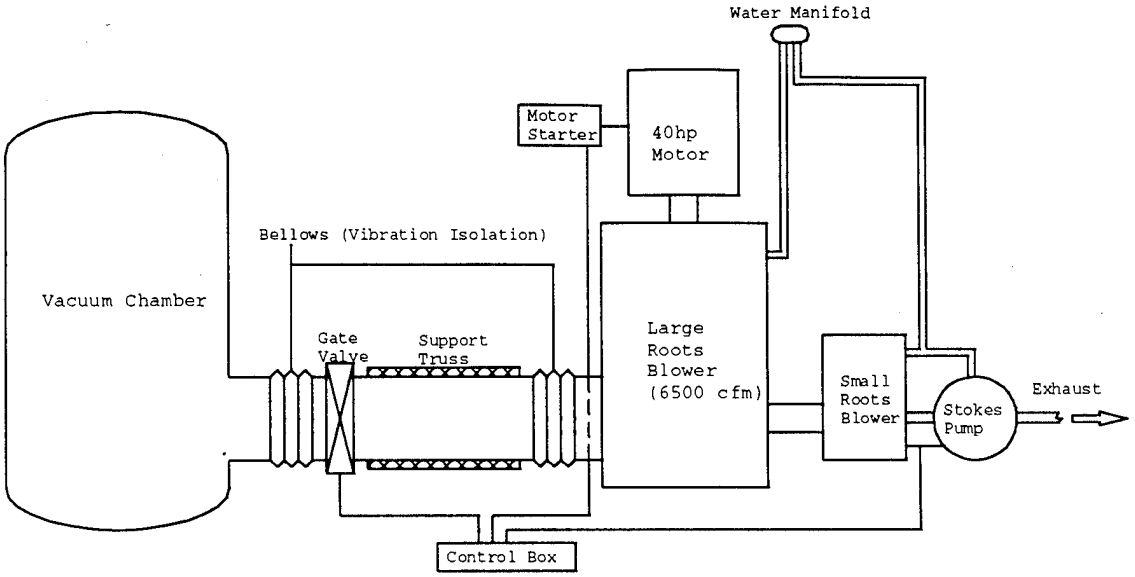

Figure 2.1. High-pump-rate arcjet test facility after refit.

2.2 Pulsed electron-beam fluorescence

2.2.1 Previous work

The pulsed electron-beam fluorescence (PEBF) technique used here is a variation on the classical technique of electron-beam fluorescence (EBF),[2.1–2.4] the standard method for species density measurements in rarefied gas flows. As will be explained, its use in the pulsed mode renders it applicable for luminous plasmas such as arcjet plumes. A brief review of EBF is now given.

A one- or two-millimeter diameter, well-collimated beam of electrons is passed through a gas flow. If the gas density is reasonably low, below that equivalent to a pressure of several torr at room temperature, an electron beam with an energy of around 30–50 keV will not be significantly attenuated over a distance of 10 or 20 cm. The beam will be visible as a thin line of fluorescence. By optical means, any place along the beam length can be selected for observation and a point measurement of the beam-stimulated emission (fluorescence) can be accomplished. The point size corresponds approximately to the size of the fluorescent cylinder that is defined by the beam and the length of the emission that is observed. The fluorescence from the selected point has properties that can be used to measure directly the local state of the gas at that point. Alternatively, the line of fluorescence may be directly imaged along a linear or planar detector to produce simultaneous measurements along the entire line.

The experimental setup for EBF is thus strikingly similar to that of laser-induced fluorescence, with the laser beam replaced by the electron beam. See figure 2.2.

The emission or fluorescence excited by an electron beam will have a spectrum peculiar to the composition and temperature of the gas through which the beam passes. It resembles the negative spectrum of a low-density gas discharge tube for a gas of similar composition. By selecting from the beam fluorescence a characteristic emission wavelength of a gas component under investigation, a measure of gas species concentration can be obtained by measuring emission intensity. The intensity is proportional to the local specie concentration over a considerable density range.

When the beam electrons excite diatomic molecules and the molecular emission bands are examined, it is also possible to obtain vibrational and rotational temperatures. This is accomplished by measuring relative intensities in the vibrational and rotational fine structure of the molecular emission excited by the electron beam. The measurements represent a direct static temperature determination, which is an extremely difficult quantity to obtain in many flow situations.

Besides these capabilities, the technique can be used to measure flow velocity and translational temperature through the Doppler effect on emission lines. Moreover, it can provide low-density flow visualization. (In the present application, of course, this feature is not needed due to the luminous character of the flow.)

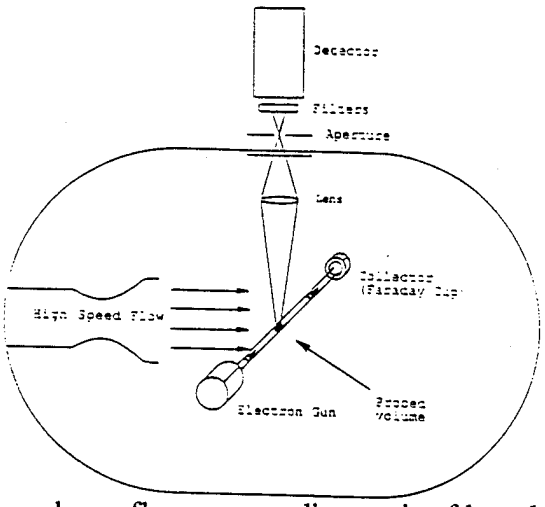

Figure 2.2. Electron-beam fluorescence diagnostic of low-density, high-speed flow.

The varied capabilities of the technique make it an attractive instrument for use in gas flows since the quantities that are measured are the undisturbed static properties of the flow, parameters that are difficult or often impossible to obtain by other means. The density range over which the technique has been used ranges from very low densities to those equivalent to a pressure of several torr at room temperature. This density range is similar to that of arcjet plume plasmas from the nozzle exit to the far reaches of the plume.

The EBF technique was used for hypersonic flow studies during the 1960s and early 70s. The technical issues surrounding its use have been discussed by Muntz,[2.1] Buetefisch and Vennemann[2.2] and Muntz.[2.5,2.6]

In this work, the propellants of interest are hydrogen, ammonia and nitrogen, as well as the atomic gases helium and argon. Of these, all have been used with electron-beam probing except for ammonia. Hydrogen, ammonia and helium are of direct interest for use as in-flight propellants. Argon's importance here is due to its excellent characteristics as a diagnostic medium as well as its high atomic weight, which renders it useful to compare with helium in mixed-propellant flows in investigating the fluid mechanics of heavy-light plasma mixtures as found in ammonia arcjets.

Nitrogen

We begin with a discussion of nitrogen. Although pure nitrogen is not often used as an arcjet propellant, it is present as a product of ammonia and hydrazine thrusters. Moreover, nitrogen has received the most use with the electron-beam fluorescent probe and hence serves as a baseline for the present application. The emissions of major importance to the technique are the first negative and second positive systems.

At low densities the most prominent feature is the first negative system (N_2^+, $B^2\Sigma \rightarrow X^2\Sigma$) of N_2^+. It can be shown that, for the first negative system, the most likely population path is the direct excitation from the neutral ground state by either primary or secondary electrons. The secondaries, in addition, populate the upper state of the

transition, giving rise to the second positive group, ($C^3\Pi_u \rightarrow B^3\Pi_g$). This system is a result of secondary electron excitation since the $C^3\Pi$ state can only be reached by an intercombination transition for the ground state.

The relative intensities in the vibrational bands of the first negative system and the relative intensities in the rotational fine structure of the system can be used to measure vibrational and rotational population distributions.[2.1]

Reliable cross sections are available for the excitation of the two brightest and most accessible band systems in nitrogen.

For pressures higher than several hundred microns of mercury, the nitrogen spectrum changes dramatically. The nitrogen first negative system begins to be quenched at a characteristic pressure $p' = 1.9$ torr for the (0,0) band. The second positive system, on the other hand, is quenched with a $p' = 35$ torr. Accordingly, the predominant emission at very high densities is in the second positive system for c-w electron beam excitation. Detailed quenching cross section for the several bands of the second positive and first negative system have been reported. The temperature dependence of the quenching cross sections is important.

Hydrogen

A spectrum of hydrogen excited by an electron beam was obtained by McCaa & Rothe.[2.7] Other rather more detailed work is available, although unpublished, and is presented here. The data and discussion that follow for hydrogen are from unpublished work of B. L. Maguire (1968). The spectra resulting from a moderately energetic (20-keV) 4-mA electron beam exciting room-temperature hydrogen at 0.6 torr was examined. The hydrogen spectrogram showed the "many-lined" appearance expected of molecular hydrogen as well as the relatively intense lines of the Balmer series of atomic hydrogen.

After comparing the hydrogen spectra and the nitrogen spectra, a wavelength region of approximately 66 Å from 4555 Å to 4621 Å was selected for observation for an emission intensity versus gas density calibration. There are at least eight relatively strong hydrogen bands in this region, with no discernible nitrogen emission intensity. There was no indication of collision quenching up to 1.1 torr (the maximum pressure reached) at room temperature.

Maguire has shown that hydrogen probing is possible using the fluorescence technique, although the cross sections for molecular excitation due to electron impact are lower than the corresponding cross sections for nitrogen. Hydrogen has not been extensively investigated in past aerodynamic studies because of its limited relevance to actual flow problems. However, this is no longer as true due to the attention being paid to hydrogen-oxygen mixing in supersonic combustion.

Helium

The strongest emission observed in the visible region when low-density helium is excited by a moderately energetic electrons is the 5015.7 Å line corresponding to the $(2^1S \rightarrow 3^1P)$ transition, which is optically allowed and thus is quite intense. Also of some interest are the lines at 4713 and 4922 Å. However, the 5016 line is used most commonly as a fluorescent probe.

In atomic work, the paucity of excited states means that account must be taken of radiative transport effects due to optical line thickness.[2.8,2.9] In helium, this has been extensively studied.[2.10–2.13] The effect is to limit the spatial resolution of EBF to about one gas atom mean free path.[2.13] This limitation is not significant for this work, however, since in expanding plume flows, the flow properties will not change significantly over a mean free path.

Argon

Argon presents several groups of emission lines that may be used in EBF probing. These include the 4277.5 and 4609.2 Å lines of Ar II as well as several Ar I lines between 7200 and 8500 Å.[2.14,2.15] In aerodynamic work, the Ar II lines are preferred since they exhibit a much smaller radiation-diffusion effect than Ar I. This is due to the much reduced self-absorption of the smaller ion population. In our case, however, we expect to be more interested in the neutral lines because of the presence in the undisturbed flow of a significant number of argon ions.

2.2.2 Present work

In PEBF, the peak electron beam current is orders of magnitude higher than in standard EBF, providing a number of additional capabilities. A high-current pulse of electrons (current ~ 100–1000 A, duration ~ 10–50 ns, energy ~ 30 keV) is used to excite fluorescence in the plume, just as in the classical continuous EBF just described. There, the electron beams are generally DC, with beam currents of order 1–10 mA. This would not be appropriate here because of the low signal level (small amount of fluorescence generated) in comparison with the highly luminous arcjet plume. By contrast, pulsed beams generate pulsed fluorescence which is instantaneously of much greater intensity than the plume, allowing gated detection with high signal-to-noise ratio.

This work used electron guns based on the pseudospark switch,[2.16,2.17] which has recently been discovered to be an efficient producer of high-emittance electron beams with the characteristics desired here. A schematic of the pseudospark switch is shown in figure 2.3. Switch breakdown causes an acceleration of electrons along the gun axis; these electrons emerge from the anode with energy roughly equal to the breakdown voltage. Collimation is very good, with beam sizes of order one-half millimeter.[2.17] The gas environment of the gun is vacuum-isolated from that of the engine test tank into which the beam passes; this isolation is not needed if the tank pressure is low (< 50 microns).

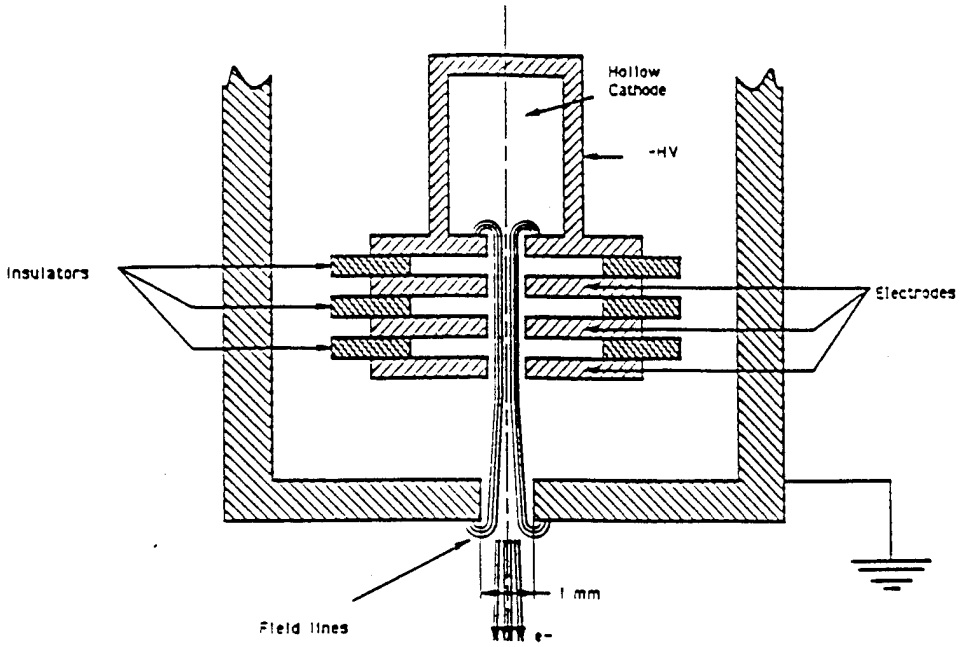

Figure 2.3. A hollow-cathode pseudospark switch.

Two electron guns, which we call "first-generation" and "second-generation," were used in this work. (The second gun was purchased from a different contract, AFOSR-URI F49620-93-1-0373.) As will be discussed, only the second-generation gun exhibited acceptable operational characteristics. The first-generation gun is shown in figure 2.4. Unlike the schematic of figure 2.3, this gun has only two electrodes, the cathode and anode. The cathode is initially held at a negative high voltage of several tens of kilovolts, relative to the anode, by charging a capacitor bank. Firing the flashlamp begins the switch closure. The discharge is triggered by photoemission due to the impingement of ultraviolet photons from the flashlamp on the back side of the cathode. The presence of significant electron population in the hollow space behind the cathode allows a long-path breakdown to occur along the field lines passing through the cathode-anode holes. This breakdown produces a short, high-current pulse of well-collimated electrons at approximately the charging voltage. Because the anode is at the same potential as the chamber, the chamber is roughly field-free and the electrons are ballistic.

The chosen design for the first-generation gun was unfortunate in that the two electrodes provided insufficient radial field line containment on axis to ensure repeatable beam formation and collimation. Because of this, the beam quality was quite poor, with considerable beam blooming at all gas pressures as well as unacceptable shot-to-shot variation.

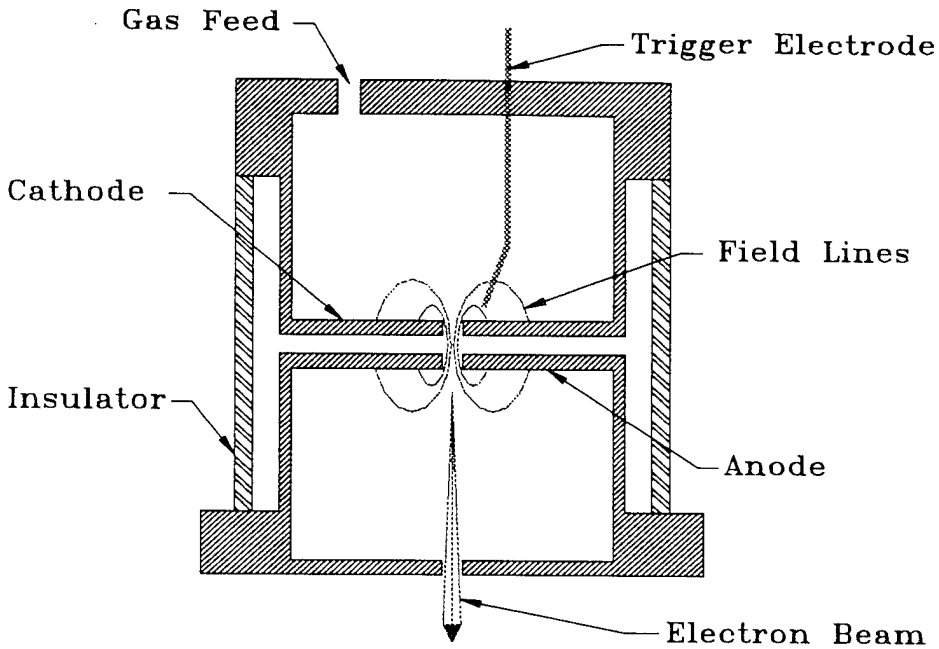

Figure 2.4. First-generation two-electrode electron gun.

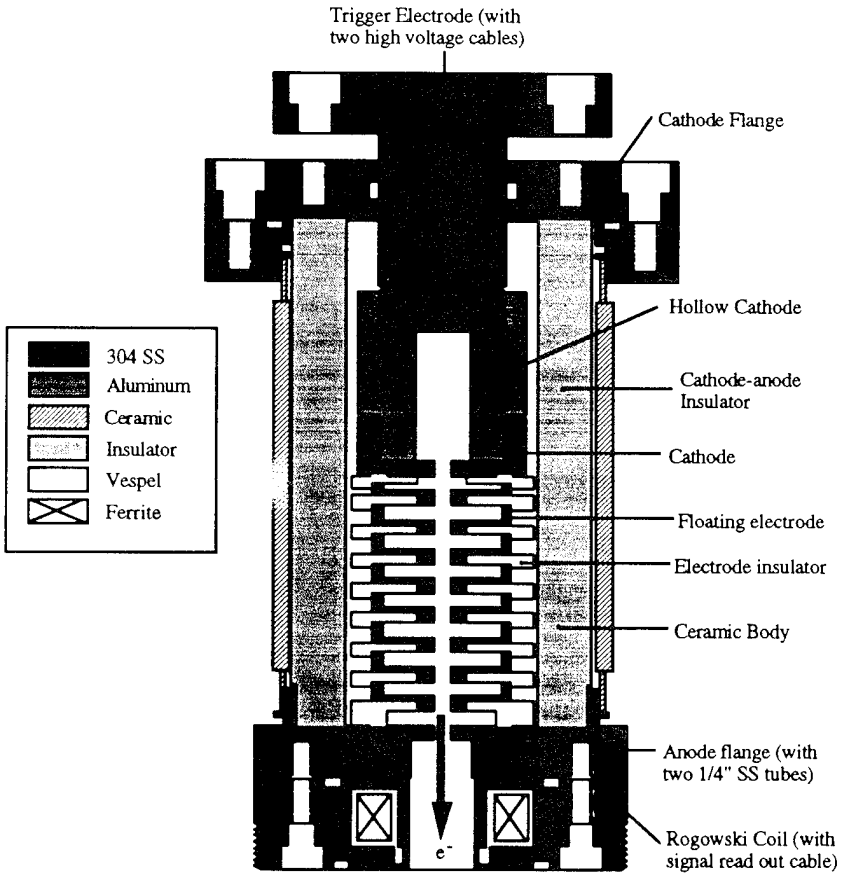

Figure 2.5. Second-generation gun. The floating electrodes are capacitively coupled during pulse charging to provide repeatable beam-forming.

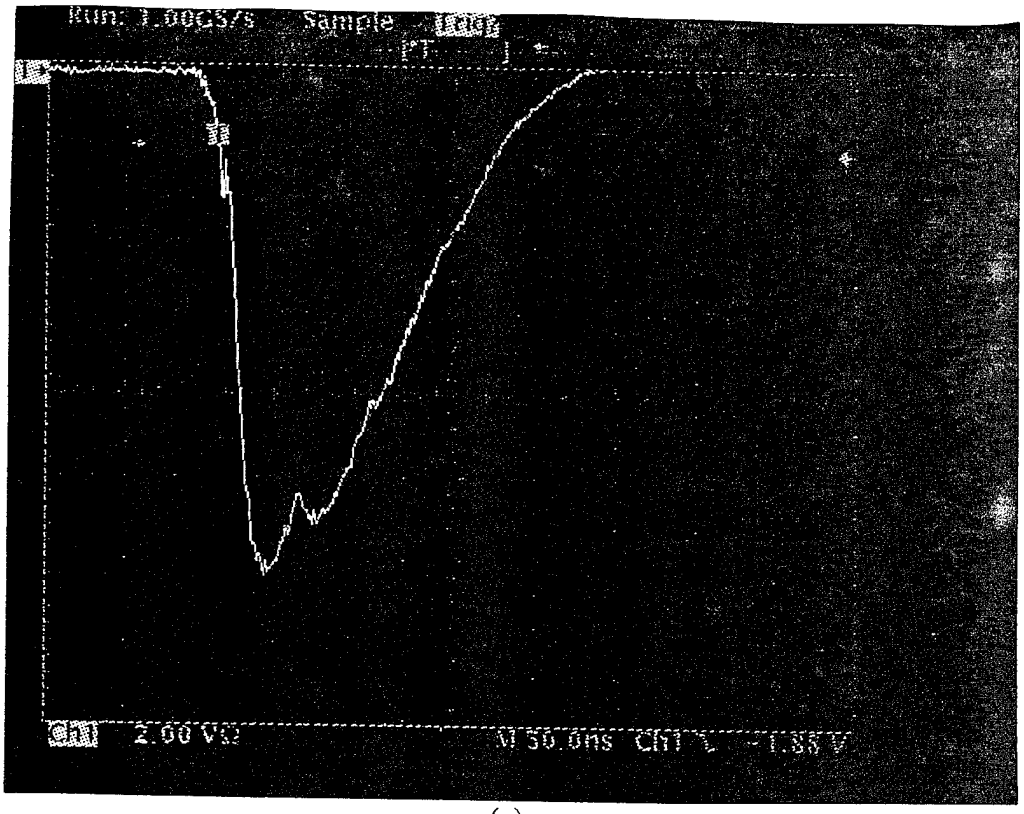

(a)

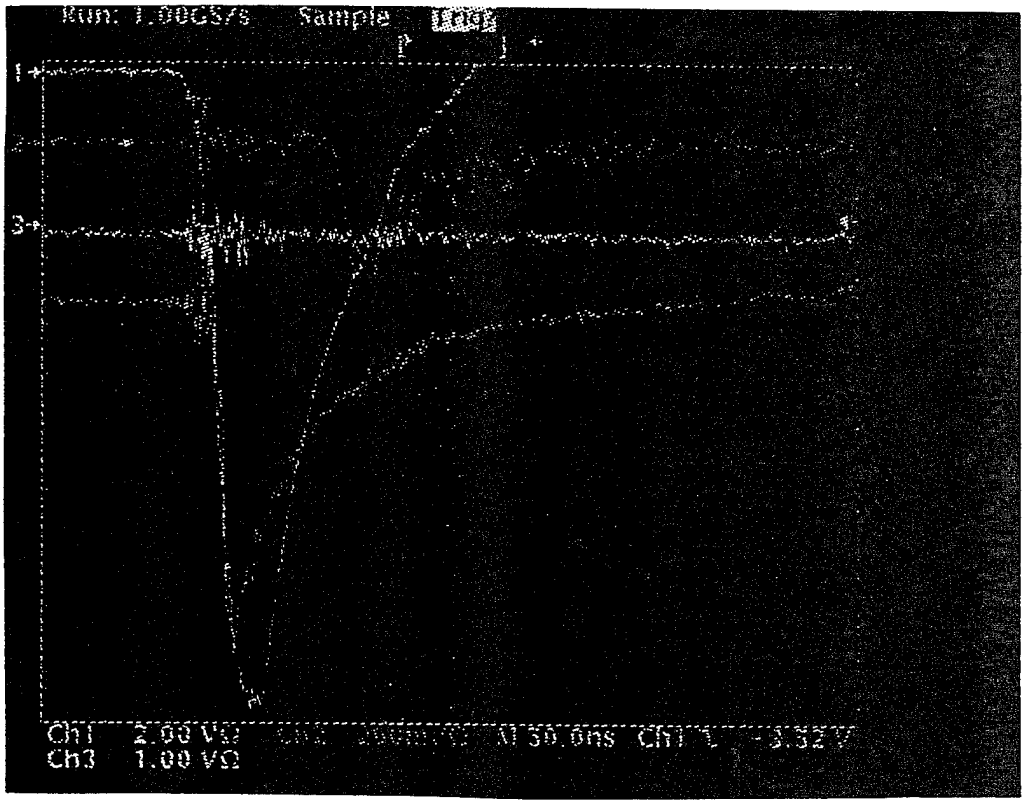

(b)

Figure 2.6. Operating characteristics of second-generation gun. Shown are beam currents at the anode (channel 1) and at a station downstream 10 cm from the anode (channel 4), for (a) hydrogen and (b) nitrogen operation. Fill pressure in all cases is 50 microns.

In order to overcome this, the second-generation gun was designed with nine electrodes with identical coaxial holes. See figure 2.5. The electrodes intermediate to the cathode and anode are floating, with dielectric spacers. The multielectrode configuration provides a substantial region of confined, uniform axial electric field under high applied voltage.

A further improvement is provided by pulse charging, rather than DC charging, the gun. A 30–45 kV pulse of several microseconds FWHM is applied between cathode and anode by a specially built thyratron-based charging circuit (not shown in figure 2.5). At the peak of the high-voltage pulse, a trigger pulse of roughly 3 kV is applied to the surface-discharge trigger. This causes the gun to fire with measured jitter of less than 50 ns, which is sufficient for time-resolved arcjet work on any realistic scale.

Pulse charging has two benefits. First, the DC voltage holdoff of the gun is no longer inportant. The operating envelope, in terms of gas composition, pressure, and beam energy, is thus considerably wider than with DC charging. Second, the intermediate electrodes, which float under DC charging, are capacitively coupled under pulse charging. The electrodes thus form a capacitive voltage divider which equalizes the interelectrode voltages and stabilizes the field for maximum beam reproducibility.

Figure 2.6 shows the operating characteristics of the second-generation gun with several gas compositions. Shown are the beam current, as a function of time, exiting the gun and after propagation over 10 cm. Note that the beam current peaks at close to 2 kA. The shortest-duration (hence probably the most monoenergetic) beams are formed during nitrogen operation.

The second-generation gun was completed and tests begun with it during the extension period at the end of this contract. For this reason, measurements of plume properties using PEBF will only be accomplished in future work and are not reported here.

2.3 Two-photon laser-induced fluorescence

2.3.1 Introduction

Recent advances in flame diagnostics indicate that methods used for observing concentrations of atomic hydrogen in flames using two photon or multiphoton laser-induced fluorescence (LIF) may be applicable to arcjet plumes. This part of the work consists of examination of these techniques and their application to the measurement of ground state hydrogen atom concentrations.

Observing atomic hydrogen during its lifetime in a non-intrusive manner often involves optical detection of the emission from radiating excited electronic states or the measurement of photon absorption through a population of atomic hydrogen. Inducing the fluorescence with laser light tuned to a specific transition frequency (LIF) can allow information on the species participating in the electronic transition to be inferred. Usually, the excited states of hydrogen are probed as the excited state transitions are more accessible to laser equipment currently available and can be detected in the visible wavelength range.

In a non-equilibrium plasma such as the arcjet plume, the excited state population of atomic hydrogen cannot be used to infer the ground state hydrogen population. Therefore, it is necessary to identify a direct method of probing the ground state of hydrogen.

In the flame environment, atomic hydrogen plays an important role in the chemistry of most combustion processes. Measuring ground state hydrogen profiles in premixed flames is considered critically important in understanding how to best model the combustion processes of flame chemistry, and the development of laser diagnostics to non-intrusively probe ground state hydrogen atoms has been explored in depth during the last decade in order to facilitate these measurements.

Research in this field has centered on three excitation schemes of ground state hydrogen: two-photon direct excitation, three-photon direct excitation, and two-step three-photon excitation. The last scheme was developed at Sandia National laboratory; work on the other two schemes has also been examined in detail at Sandia as well as at numerous other institutions. An overview of these schemes is given in the following sections.

Researchers at Sandia[2.18–2.26] examined the uses of multiple-photon stimulated emission to promote ground state radicals to an excited state whereby emission in the visual wavelength region could be detected. Problems inherent in the technique were investigated and included the dependence of the emission signal on three parameters: laser power, ambient gas pressure, and the spectral shape of the stimulated emission. Multiple photon excitation schemes were found to have increased sensitivity to each of these parameters as compared with standard single photon laser induced fluorescence.

Taking this diagnostic approach to the hydrogen atom was demonstrated using a two-step method where a two photon transition was used to excite the ground state of hydrogen to the first excited state (n=2) and then a resonant detection scheme, requiring a second laser, excited some of those placed in the first excited state to the second excited level (n=3) via a single photon transition. The resulting decay from n=3 to n=2 is observed.

The n=1 to n=2 transition requires a single photon at a wavelength of 121.5 nm or a two-photon transition at 243 nm (the absorption cross-section for a two photon transition is substantially smaller than for a single photon transition and will be discussed later). The latter wavelength is more desirable for two reasons. The 243 nm light is much more easily created with the laser technology available today (including doubling/tripling crystals and pressure cells) and wavelengths below 200 nm are easily absorbed by the atmosphere and require a vacuum path for the entire path of the beam.

To complete the two-step method mentioned above, an additional 656 nm beam promoted those atoms that were previously excited (based upon the cross-section probability) to n=3. Subsequent detection of 656 nm emission is observed.

Comparison of this technique with direct two-photon and three-photon schemes was conducted by researchers at Sandia and found to provide more accurate results for rich hydrocarbon flames, though almost identical results for most simple flames. The two step technique may be more difficult to implement than the other techniques as it requires two lasers (though a variation using different transitions can make be accomplished with only one laser) making the experiment more complex and costly.

One of the side effects of the multiphoton direct excitation techniques in hydrogen is that they directly promote ground state electrons to the second excited level thereby causing a potential population inversion between the first excited state and the second excited state. This takes place only along the line of irradiation by the ultraviolet laser beam (typical for irradiation of ground state hydrogen atoms) and can lead to the creation of an additional laser beam (in the visible for hydrogen when, for example, Balmer α radiation is initiated) along the path of the initial beam. This reabsorption of emitted photons can cause a problem if a measurement is attempting to create an analog between light collected and the density of emitters and must either be accounted for or avoided.

Researchers at Sandia were the first to examine this optically excited stimulated emission (sometimes called amplified spontaneous emission or ASE) and its relationship to the multiphoton fluorescence diagnostic. One of the important observations was that while the fluorescence due to the excitation followed a laser power-squared behavior, the ASE fluorescence went as laser energy to a higher exponential power meaning that it could dominate at higher laser energies and drop to an insignificant process at lower laser energies.

Using the ASE as a diagnostic itself was examined, but its line-of-sight nature and the requirement of transition saturation before a linear relation between species density and signal is observed led to difficulties in application.

In order to use the multiphoton diagnostic technique as a measure of atomic hydrogen density a correlation between the number of emitters and the measured fluorescence is required. A process which can prematurely depopulate atoms excited by the diagnostic is collisional quenching due to even a moderately high pressure environment. Sandia has looked at the time-resolved fluorescence decay of the atomic hydrogen in low pressure flames (20 mTorr or ~3 Pa) to examine the relationship of pressure to quenching for this diagnostic technique and has characterized the relationship between the fluorescence decay times and the expected attenuation of the emitted fluorescence. Changes in pressure, and correspondingly in quenching, can be determined through observation of changes in fluorescence decay times of the LIF.

Relative hydrogen density measurements were compared with flame models using these techniques and the results were found to agree well. No calibrated atomic hydrogen density measurements were made at Sandia to our knowledge.

At the University of Stuttgart,[2.27-2.30] detailed examinations of quenching, excitation linewidth, and fluorescence calibration for two-photon LIF diagnostics on atomic hydrogen in flames have been performed. Direct two-photon laser induced fluorescence at 205 nm was implemented to promote ground state hydrogen atoms to the n=3 excited state where n=3 to n=2 (Balmer α) fluorescence was observed. Key to the work performed at Stuttgart was detailed calibration of the fluorescence using a calibration cell containing atomic hydrogen created from a microwave discharge. Hydrogen densities in the cell were determined using a chemical gas titration technique that is discussed later in greater detail.

Additionally, the technique was successfully demonstrated near a heated filament where pressures ranged from 1 to 100 mbar (100 to 10,000 Pa) and the hydrogen source came from a 5% CH_4 chamber environment. Quenching effects were calculated in pressure ranges above 10 mbar and determined from fluorescence lifetime decay rates at lower pressures as described earlier.

Ohio State University[2.31,2.32] also has done several multiphoton LIF experiments similar to the groups discussed previously. Of interest in this work is additional attention to detail involving chemical titration calibration of two-photon LIF and corrections for collisional quenching. Atomic hydrogen density is determined in a calibration cell using titration of small amounts of NO_2 to chemically react with hydrogen atoms present in the cell. Additionally, the fine structure of the n=3 state of atomic hydrogen was examined in order to determine the unquenched radiative lifetime of this excited state when populated by a two-photon excitation process. This lifetime is important in determining the correction factor applied to a quenched signal through measurement of fluorescence decay.

Kyushu University[2.33,2.34] has closely compared four different two-photon excitation schemes. They found that unless hydrogen densities are very low ($<10^{11}$ cm^{-3}), losses in detecting vacuum UV emission require the use of fluorescence emission in the visible to detect hydrogen atoms and this constrains the choice of excitation level to either the n=3 or n=4 excited state. Of these options the Kyushu group determined that two-photon excitation into the n=3 level and the subsequent observation at the Balmer α wavelengths produced the largest number of fluorescence photons per incident laser photon. This also was the best choice if molecular dissociation due to the incident laser was to be avoided and if incident intensities were to be kept low (to avoid ASE, for example). In addition, two photon excitation from n=1 to n=3 also appeared to be the least sensitive to collisional quenching of the four techniques that were examined. Due to all of the above advantages, it appeared that for an environment somewhat similar to that in electric propulsion plasmas, the two-photon to n=3 scheme appeared to be the technique of choice.

2.3.2 Laser-induced fluorescence — general discussion

LIF spectroscopy has gained wide acceptance in the past two decades as a diagnostic technique that generates measurable fluorescence from a small species population that otherwise might not be detectable.[2.35] Fluorescence, the spontaneous emission of radiation from upper energy levels, is observed when a population increase of an upper level is created through photon absorption, particle collision, or many other interactions, and then emits photons as the level relaxes to a lower population (see figure 2.7). Increasing the population of selective upper levels can be obtained by exciting specific lower levels of the species with coherent light of fixed frequency. This excitation process (usually accomplished with laser light) can increase the population of the upper level for a set duration based upon the population of the lower level. Fluorescence resulting from the increased population during the pumping time is often significantly larger than without the excitation pumping and thus provides a means of observing small species populations and allows investigation of the populations of the lower energy levels that are used to supply the upper levels.

Laser light used for the excitation process must be of the specific frequency that corresponds to the energy difference between the lower and upper levels of the transition being probed. In order to create laser light at the specific frequency required for many different transitions, tunable dye lasers are often employed to allow probing in the range from 200nm to 1.5mm. Probing in regions around and below 200nm is often difficult due to atmospheric absorption, but can be avoided through the use of multi-photon processes.

Multiple photons of a frequency related to a transition spacing by an integer multiplication, can induce the transition to take place. A weaker excitation cross section is typical for multi-photon transitions when compared to the cross section for the transition with single photons.

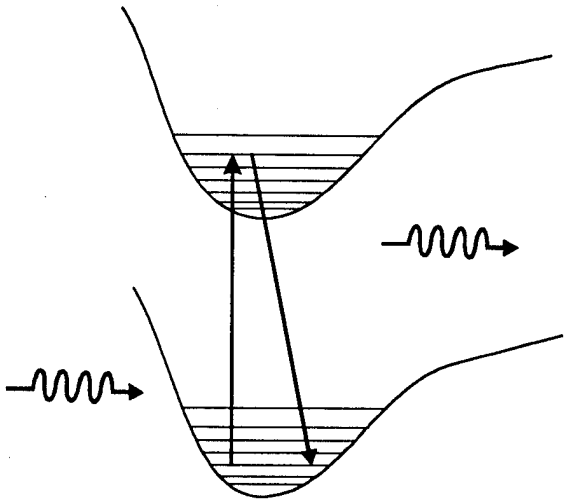

Figure 2.7. Interaction (in this case an absorption of an incoming photon) with a molecular or atomic species can cause an excitation of an electron in a lower electronic state to be excited to an upper state and consequently emit a photon of a frequency corresponding to the transition of relaxation back to the lower level.

To perform LIF (with single or multiple photon transitions) on a particular species several criteria must be met. The molecule or atom in question must have a known emission spectrum so that the fluorescence detected from the excitation can be properly accounted for. Processes such as dissociation from the excited state can affect the fluorescence that is measured and sometimes even prevent it from being detected at all. This is also important if the fluorescence produced from exciting the species is to be related to the intensity of the pumping or the density of the species in the lower levels.

As previously discussed, methods for creating the light needed to pump the transition must also be available. Tunable coherent light sources are desired for use in LIF due to the need to both match frequencies to atomic and molecular transitions and to scan across the transition frequencies in order to learn information about fine structure, intensity, linewidth, etc. In different spectral ranges, different tuning methods have been developed to initiate the desired light. Devices spanning these ranges include semiconductor diode lasers, tunable gas lasers, pumped dye lasers (both pulsed and continuous wave), and excimer lasers.[2.36]

The radiative decay rate from the upper excited state must be known as the fluorescence power is proportional to that rate.[2.35] Also, as other species are present, a decrease in excited state population may occur due to factors other than spontaneous emission such as collisions and laser-induced chemistry. These quenching processes must be accounted for in order to correct the measured fluorescence so as to determine species number density.

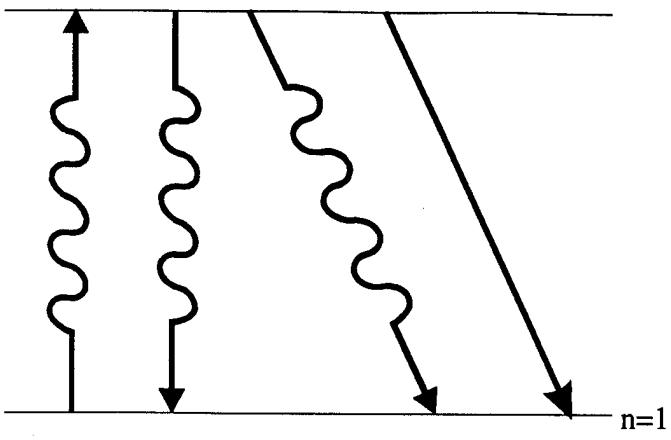

Figure 2.8. Two-level energy diagram showing excitation and relaxation processes.

In the simplified case of a two level energy system with a lower level (n=1) and an upper level (n=2), the rates for the optical and collisional processes connecting the two levels (figure 2.8) can be described by four processes and their rate coefficients: stimulated absorption (b_{12}), stimulated emission (b_{21}), spontaneous emission (A), and quenching (Q_{21}). The Einstein A and B coefficients are related to these rates in the following manner. The spontaneous emission is given by the A coefficient and the stimulated rates are related to the B coefficient through the following expression (degeneracies of the levels are ignored):

$$b_{12} = b_{21} = \frac{BI_\nu}{c} \tag{2.1}$$

where I_n is the spectral irradiance which is defined as the incoming laser intensity per unit frequency interval and c is the speed of light. The stimulated rates are therefore a function of the incident laser intensity, linewidth, and pulse duration in addition to the nature of the species transitions in question.

The rate equations for the change in population of the two states can be written utilizing these four parameters and the populations of the respective levels N_1 and N_2:

$$\frac{dN_1}{dt} = -N_1 b_{12} + N_2 (b_{21} + A + Q) \tag{2.2}$$

$$\frac{dN_2}{dt} = +N_1 b_{12} - N_2 (b_{21} + A + Q) \tag{2.3}$$

(2.2) and (2.3) allow the determination of each level's population. For the closed-system case examined, the population rate equations could be coupled assuming population conservation. By substituting for N_1 and then integrating, a relation for the upper state population based upon an exponential term in time results,[2.35] given by

$$N_2 = \frac{b_{12} N_T}{b_{12} + b_{21} + A + Q}\left(1 - e^{-(b_{12}+b_{21}+A+Q)t}\right) \tag{2.4}$$

As the exponential approaches a steady state (as the exponential term in time becomes greater than one) the population of the upper level approaches the constant value

$$N_2 = \frac{b_{12} N_T}{b_{12} + b_{21} + A + Q} \tag{2.5}$$

where N_T is the total population and is equal to the sum of the initial populations. This can be rearranged, using (2.1), to

$$N_2 = N_T \left(\frac{b_{12}}{b_{12} + b_{21}} \right) \frac{1}{1 + \frac{A+Q}{b_{12} + b_{21}}} = \frac{N_T}{2\left(1 + \frac{I_\nu^{sat}}{I_\nu}\right)} \tag{2.6}$$

where the saturation spectral intensity I_ν^{sat} is defined by

$$I_\nu^{sat} = c \frac{A + Q}{2B} \tag{2.7}$$

Thus, for the closed system case, after a time greater than the exponential characteristic time, the upper level population can be described by the ratio of spectral intensity to its saturation value.

Another approach for a more realistic system is to assume a steady state in the population of two levels and solve for the population by setting the two rates equal to zero. However, a steady state may not be achieved when laser pulses are short and laser intensities are small such that quenching processes dominate.

The fluorescence observed is given by the population of the upper level, the spontaneous emission rate, the frequency of the emitted photon, and the physical irradiation volume of the laser light:

$$F = h\nu N_2 A \frac{\Omega}{4\pi} V \tag{2.8}$$

where $h\nu$ is the photon energy, Ω is the collection solid angle, and V is the volume comprised of the focal area of the laser beam and the length over which the fluorescence is observed. For a given optical setup probing a given transition of a particular species, the fluorescence varies only with N_2..

2.3.2.1 Two-photon excitation of hydrogen

Transitions of interest are often found where excitation would require photons with a wavelength below 200 nm. Not only is excitation of these transitions difficult due to the absence of tunable wavelength lasers available in this range, but it is also difficult to implement due to the strong absorption at these wavelengths by the air in the laboratory and by other gases that may be present inside a test facility. Consequently, when transitions below 200 nm are intended to be pumped, a multiphoton approach (usually two or three photons) is used. Two-photon cross sections are quite small. However, photons with half of the frequency or double the wavelength can be much easier to create in the laboratory. Stimulated emission of an atom that has been excited by the two-photon process can be neglected. For a two-photon process, (2.3) becomes

$$\frac{dN_2}{dt} = +N_1 W_{12} - N_2 (A + Q), \tag{2.9}$$

where W_{12} is the two-photon cross section.

Two-photon cross sections have been measured and reported in literature[2.35] and cannot be directly related to single-photon cross sections due to their representation of different processes and different units. As a rough rule of thumb, under common conditions an order of magnitude more laser intensity is required for signals similar to standard LIF when using a two-photon scheme on atomic species in an atmospheric flame.

Fluorescence due to a two-photon absorption is quadratically related to laser power, while the excited state population is affected by quenching linearly as in single-photon fluorescence.

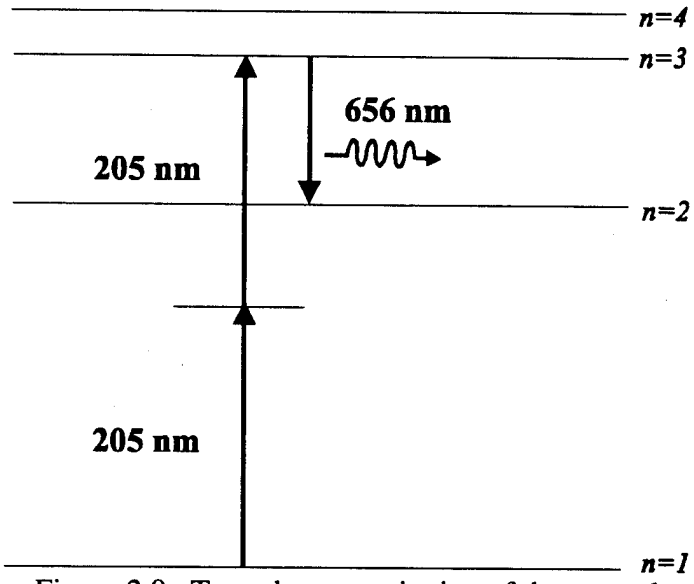

Figure 2.9. Two photon excitation of the ground state hydrogen atom to n=3 and the resulting fluorescence (not to scale).

The specific problem of excitation of the ground state of hydrogen to its excited states requires a single photon below 200 nm or a two-photon excitation using wavelengths that are greater. Since this excitation is intended for use as a diagnostic technique, detection will be important so excitation to the second excited state (n=3) or third excited state (n=4) will be desired as relaxation to the first excited state from either of these states can be detected in the visible wavelength range (656 nm for n=3 → n=2, 486 nm for n=4 → n=2) . Excitation to the second excited state of hydrogen and the resulting fluorescence is shown in figure 2.9.

One-photon excitation to the second excited state requires photons of wavelength 102.5 nm, while a two-photon transition requires wavelength 205 nm, much more easily created in the laboratory through doubling or tripling of 410 nm or 615 nm laser light which is readily available using tunable dye lasers.

One of the problems of the scheme of figure 2.9 is the population inversion created between the first and second excited states when directly pumping ground state atoms to the second excited state. This inversion serves as a gain medium for the 2–3 transition along the path of laser stimulation. The resulting amplified spontaneous emission (ASE) complicates the interpretation of the fluorescent signal, and can actually create a new laser beam in the hydrogen being probed along the path of the 205 nm two photon excitation beam.[2.23]

2.3.2.2 Three-photon excitation of hydrogen

There have been reported two methods of exciting the ground state of atomic hydrogen involving three-photon excitation. One involves populating the first excited state with two photons and then populating the second or third excited state with a photon of another wavelength, thus avoiding the population inversion problem and ASE. Another three-photon method involves directly populating the second excited state with three photons of the same wavelength.

Two-step LIF on ground state hydrogen atoms uses two 243 nm photons to promote ground state atoms to the first excited state, while a second photon at either 486 nm or 656 nm excites the atom in the first excited state to the third or second excited state respectively. This is shown in Figure .

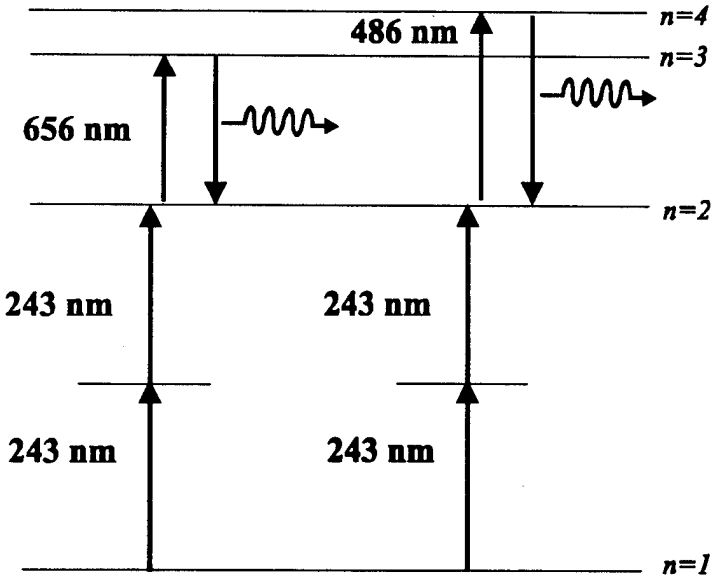

Figure 2.10. Two-step, three-photon excitation schemes (not to scale).

These techniques are more difficult in two respects. First, two-step excitation requires resonant detection. In other words, the light being detected is at the same wavelength as one of the laser beams and cannot be spectrally separated. The fluorescence is only separated temporally from the laser beam on a timescale related to the Einstein coefficients of the depopulation of the chosen excited state. Scattered laser light can interfere with measurement of the fluorescence signal especially in low-signal situations and make

detection extremely difficult. Second, both techniques require a second photon to continue the excitation process once the first excited state is populated. This requires the two lasers to overlap the detection area both spatially and temporally in order for the full excitation to occur. In the case where the second step is accomplished by a 656 nm photon, a second laser is required. If a 486 nm beam is used, one laser can produce 486 nm and some part of the beam can be doubled for 243 nm. This requires only one laser, though it must have enough energy per pulse to support each of the transitions in the environment being probed. This method is called single-laser two-step excitation and is the preferred implementation of the two-step techniques.

Two-step techniques avoid population inversions associated with other two and three photon excitation schemes, but add an additional layer of difficulty in both implementation and understanding of what is being probed. Instead of exciting the ground state directly to a level where fluorescence takes place, two-step excitation excites atoms to an intermediate level where they are then excited again at some rate to a higher excited state. If density measurements are to be made using this technique a method for understanding the total cross section of the excitation must be developed. Promotion to the final excited level occurs according to the convolution of the two laser lineshapes. This becomes even more difficult if the gas being probed is moving at high velocities (~ km/s) with respect to the incoming photons, so that Doppler shifts are significant, as in the arcjet plume environment. The first beam will excite atoms based upon their relative velocity as well as density, while the second beam will also excite some part of those by velocity from a group that has already been selected by velocity. Tying the laser scan rates together by wavelength (or using one laser for both beams) may allow this problem to be overcome.

As previously mentioned, there is another scheme found in the literature that involves using three photons to probe ground state hydrogen atoms. Three photons at 292 nm together excite the ground state to n=4 where n=4 to n=2 fluorescence is observed. This method has not been deemed very practical due to the even smaller cross section for three-photon excitation than for two-photon excitation and it does not deal with the ASE issue any better than two-photon excitation to n=3. Additionally, when compared to the previously mentioned excitation schemes it is found to have lower signal to noise than the others. It does have the benefit of using the highest wavelength photons which are more easily created in the laboratory.

2.3.3 Detecting hydrogen atoms in an arcjet plume

Of the techniques described above, the two that appear to be of most interest are two-photon direct excitation of the second excited state and single-laser two-step three-photon excitation to the third excited state. These techniques have been shown to adequately probe the flame environment for ground-state atomic hydrogen. They appear to be the best candidates to measure absolute density of hydrogen in an arcjet plume. The present work employs the two-photon direct excitation method. Future work may shift to the

other technique should ASE and other properties unique to this method prove to be insurmountable.

These diagnostics can also determine velocity and temperature of the ground state hydrogen in the arcjet plume using nearly the same experimental setup as for density measurements.

This point specific diagnostic technique requires that at minimum, accurate spatial alignment between one laser beam and an optical detection train be maintained. Depending upon the excitation technique, multiple pulsed beams are required to be aligned, not only spatially, but also temporally. Furthermore, at least one of the laser beams is in the ultraviolet spectrum and is not visible.

In order to satisfy this requirement a target made of a pointed metallic rod is attached to the three dimensional translation stage the arcjet is mounted on and set a fixed distance away from the center of the arcjet nozzle exit. For alignment of the laser beams, the rod is moved to the location the detectors observe and the beams are aimed onto the rod. Scattering off of the tip of the rod is visible to a photomultiplier detector with spectral filtering removed. Observing the signal intensity on a fast oscilloscope, temporal alignment is made. Differentiation between laser beams is be made by blocking one or the other and observing the signal on the oscilloscope. The effect of the ultraviolet beam on the end of the metal rod can be seen as a spark with the present laser equipment, and the ultraviolet beam can be seen to fluoresce on a high cotton content business card (many different cards have been tested and there is an amazing difference between them). After alignment, the motion-control axes are returned to their arcjet-centric home position. Absolute position within the arcjet plume cannot be made even with respect to arcjet nozzle position, so scanning through the plume in each axis is required to determine plume center and nozzle exit location.

Velocity measurements of the plume are taken with respect to the laser beam's orientation. Accordingly, two laser beam paths are used to measure axial velocity (beam shining into arcjet nozzle) and radial/azimuthal velocities (beam shining perpendicular to nozzle exit normal vector).

Because these techniques are very sensitive to laser power, strict control over laser power must be maintained. Power measurements are made regularly between scans to verify constant laser power, while pulse-to-pulse measurements during the scan are used to calibrate intensity data.

Detection of the fluorescence in the bright arcjet plume is a difficult problem and is one of the driving factors on laser power. Increased laser power increases fluorescence for a given density of atoms in the probe volume and allows the signal to more easily be observed over the background radiation, but also leads to multiphoton ionization, ASE, and saturation, which must be avoided in order to accurately interpret the signal. Efficiency in signal collection is thus required.

Because the PMT is continuously exposed to the luminous plume radiation, the average current in the dynode chain is quite high. Under typical conditions, the PMT current-source circuitry is thus close to saturation. This is avoided by the use of a gated PMT socket (Hamamatsu) which is gated on only during a narrow window around the LIF events. This provides an increase of roughly an order of magnitude in effective sensitivity, as the cathode voltage can be higher than without the gated socket.

To most efficiently collect light from the arcjet plume, a lens is placed as close as possible (without it or its mount melting) to the arcjet nozzle exit. The lens collimates the collected light and a second lens focuses the light on to the PMT. Bandpass interference filters are placed in front of the PMT outside of the chamber. Signal from the PMT is digitized by a digital oscilloscope for purposes of determining signal lifetime or laser pulse width or collected by a gated integrator to amplify and average the signal from shot to shot.

Accurate understanding of the collection volume is important. The collection volume is the intersection of the laser beam cross section with the detection focus cross section. Determining the size of the laser beam at the point of the detection is important for this calculation and is accomplished by imaging the beam onto a photodiode near the collection volume with the laser source on the other side of the collection volume. A razor blade is passed through the collection volume attached to a motion control stepper motor system. By slowly moving the razor blade through the beam the size of the beam from fully blocked to not blocked may be determined. Assuming a Gaussian laser shape, the beam waist can be determined from half of the trace of intensity vs. position.

A light source may be placed in the PMT housing with the tube removed so as to image light to the collection volume back along the optical train. This can also be measured in the same fashion and the intersection of the two measurements defines the collection volume.

To make spatial profiles of atomic density in the arcjet plume the diagnostic must be applied to several locations across the nozzle exit of the 1 kW hydrogen arcjet. Rather than moving the entire optical detection train and the laser optics, movement of the thruster itself on a three-dimensional motion control axis is chosen. This allows the optics to remain fixed once aligned. To interpret axial position data, the nozzle exit is considered to be the point where signal drops to half of what it was before approaching the nozzle exit. This assumes that there are not significant drops in atomic hydrogen as one gets closer to the nozzle exit.

To accurately differentiate density, temperature, and velocity measurements, Gaussian profiles are least-squares fitted to spectral profiles at each spatial location in the plume where density is to be measured. (We find that modeling using Lorentzian or Voigt profiles is insignificantly different than Gaussian.) This allows accurate determination of line centers, line widths, and line areas. Each measured profile is fit to a Gaussian using a

Levenberg-Marquardt least squares fit.[2.37] The wavelength shift of the center of the line profile with respect to the line profile of a stationary gas simultaneously probed yields the axial velocity when the laser beam focuses down the axis of the thruster into the nozzle and the radial or azimuthal velocity when the beam is perpendicular to the nozzle exit normal vector. The width of the Gaussian profile can then yield the temperature of the gas.

Density measurements are made based upon accurate integration of the absorption lineshape of the transition that is probed. Fluorescence signals from different parts of the arcjet plume as well as a calibration environment (discussed below) are related to each other for relative and absolute density measurements. This can only be successful if the integrated fluorescence in each area of the plume (and calibration cell) is understood with respect to the appropriate broadening mechanisms and artificial depopulation mechanisms taking place at different spatial locations in the plume.

One line-broadening mechanism that must be addressed is saturation broadening due to high laser energies. This mechanism can be observed (along with other mechanisms described below) when the integrated fluorescence signal deviates from the power-squared relationship between laser power and total fluorescence present.

A small amount of line broadening is caused by the linewidth of the dye laser beam which, unlike that of continuous wave ring dye lasers, is non-negligible compared with the atomic linewidth. The laser linewidth of the available dye laser when tripled to 205 nm (for the two photon direct technique) has been measured by taking an LIF spectrum of NO gas in a calibration cell. Since NO is much heavier than hydrogen, and is at room temperature, the width of the rotational lines in the LIF spectrum reflect only the linewidth of the laser (as long as care is taken to use unblended rotational lines). This has shown that the laser has a width of 0.28 cm^{-1} or 0.012 Å at 205 nm. The effect of the laser width is taken into account using the following relation:[2.38]

$$\Delta\nu = \sqrt{\Delta\nu_D^2 + 2\Delta\nu_l^2} \tag{2.10}$$

where $\Delta\nu_D$ is the true Doppler width of the line (in cm^{-1}), $\Delta\nu_l$ is the width of the laser, $\Delta\nu$ is the measured transition width, and the factor of two is due to the two-photon probe method.

Stark broadening mechanisms will also be present in the arcjet plume and need to be understood and quantified. Stark broadening is not expected to affect the density measurements significantly and are expected to be of greatest concern for temperature measurements where the temperature is determined as related to linewidth squared. A more detailed discussion on the effects of Stark broadening is given below as it relates to the overprediction error in measuring temperature due to unknown electron densities.

When looking at the total convolved lineshape, the Doppler broadening component (as will be seen below) dominates and the Stark component is minimal. If the laser linewidth is deconvolved from the total linewidth before modeling, and the laser power is kept low

enough to avoid saturation, a Gaussian profile with the appropriate uncertainty due to Stark effects appears to adequately model the transition linewidth.

The arcjet plume environment has substantial density gradients as the plume expands from the thruster nozzle exit. The changes in density with respect to position result in changing effects of depopulation of excited state hydrogen atoms due to collisional quenching. Correction for the quenching rate at the location of the measurement must be made.

One method of determining the quenching correction is to determine the effect of quenching through observation of the lifetime of the fluorescence signal on a fast 500 MHz digitizing oscilloscope. The lifetime of the transition can be determined by finding the $1/e$ time of the exponential decay of the fluorescence observed. The measured signal decay is a convolution of the laser pulse decay and the transition decay and must be deconvolved prior to the measurement. Relating the lifetime at each point in the plume to the unquenched lifetime gives a linear correction factor for the measured integrated fluorescence at that point and the effective unquenched signal can be determined in order to determine a relative density measurement. Calibration of the signal is required to convert the relative density measurement to an absolute number density. At the moment it is premature to determine expected density error as the number of contributing factors is large and the error in many of the factors (including calibration) have yet to be determined.

A focused pulsed laser beam creates a very high instantaneous energy density, which is needed to excite the two-photon transition, but also may induce other non-linear processes. Multiphoton ionization (MPI) will occur, and partial saturation of the transition becomes possible, even though the two-photon absorption cross section is very small. In addition, amplified spontaneous emission (ASE) will take place for the direct two-photon excitation technique, since a population inversion is created between the pumped n=3 level and the nearly empty n=2 level. The population inversion can cause gain to occur for any photon emitted in the forward or backward direction along the laser beam.[2.24,2.39,2.40] If ASE or MPI become large, they become a non-negligible loss mechanism for the LIF process. Saturation will cause power broadening of the Doppler profile of the transition, and saturation, ASE or MPI will cause the power dependence of the LIF signal to deviate from the expected behavior proportional to power squared.

A preliminary laser study shows that the fluorescence signal in the arcjet plume follows power squared behavior at low laser powers and deviates substantially from the power squared correlation at laser powers higher than 0.05 mJ per pulse. Finding a way to detect the fluorescence in the plume accurately enough for detailed spectral profiles while remaining at these low laser powers will be of great importance in avoiding saturation, MPI, and ASE.

Temperature measurements are based upon accurate determination of the Doppler line broadening due to thermal gas motion. Understanding the component of linewidth directly associated with Doppler broadening is essential for temperature determination.

Temperature is based upon the square of the measured Doppler width and can be written in terms of width in the following manner (SI units):[2.36]

$$\delta\lambda = 7.16\times10^{-7}\lambda_0\sqrt{\frac{T}{M}} \tag{2.11}$$

where $\delta\lambda$ is the linewidth due to Doppler broadening, λ_0 is the line center, M is the molecular weight of the gas, and T is the translational temperature. Note that when solving for the temperature based upon the Doppler linewidth, the width is squared and any error associated with the measurement of Doppler width is also squared. Because of this relationship, it is expected that error in measurement of temperature may be significant and could be ± 30% based on preliminary findings.

One broadening mechanism that will be present and must be taken into account for accurate determination of Doppler line widths is Stark broadening of the desired atomic hydrogen transition due to the free electrons present in the arcjet plume. We do not have any direct measurement of the profile of the electron number density for our arcjet, but it has been measured for nearly identical conditions[281] to be less than 2 x 10^{15} cm^{-3} at maximum in the center of the nozzle exit plane. This value of n_e would cause a Stark width of 0.002Å for the Lb line.[2.41] A simulated Voigt profile using this Lorentzian width shows that, for a typical measured linewidth of 0.029Å, accounting for the Stark broadening would cause the temperature from the Doppler portion of the linewidth to go down from 1600K to 1490K. This represents a likely maximum uncertainty in our temperature due to Stark broadening, and will be greatest at the center of the nozzle where n_e is largest.

Velocity is measured by observing the Doppler shift of the absorption line and determining the velocity relative to the incoming photons responsible for the shift:

$$v = \frac{\Delta\lambda}{\lambda_0}c \tag{2.12}$$

where v is the velocity, $\Delta\lambda$ is the wavelength shift, λ_0 is the zero velocity line center, and c is the speed of light. Determining the line center of a profile with the Gaussian fitting process discussed above is relatively simple. Performing the procedure simultaneously on both a static gas in a calibration cell and in the arcjet plume provides a shifted Gaussian in the arcjet plume and a calibration of zero velocity in the calibration cell. Determination of the shift between the two profiles $\Delta\lambda$ allows the use of (2.12) to determine gas velocity.

In arcjet plumes, velocity of species has been seen to vary from 5 km/s to 15 km/s using the above technique with accuracy as high as 50 m/s with continuous wavelength lasers and accuracy somewhat less resolved with pulsed lasers. In this case resolution is a factor of six less than typical LIF velocity measurements which probe the excited state at 656 nm as the transition being probed has an effective transition wavelength of 102.5 nm. Even with this constraint, velocity measurements of the ground state should still be quite resolved with resolution expected to be about 500 m/s.

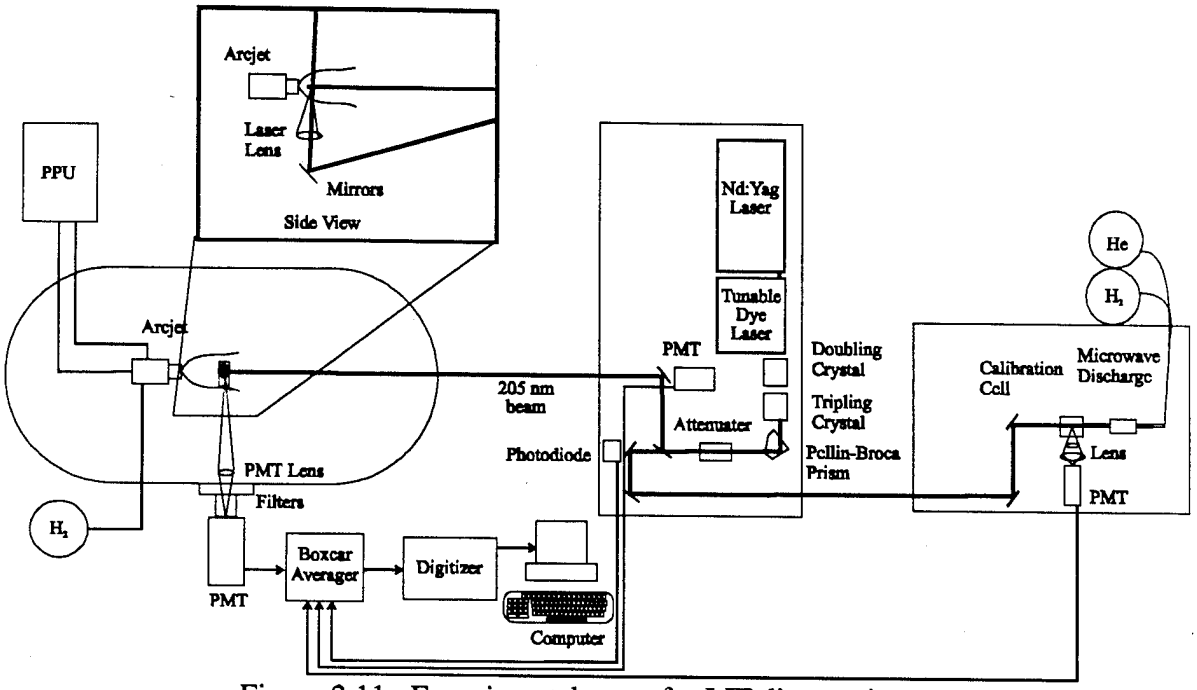

Figure 2.11. Experimental setup for LIF diagnostics.

The experimental setup is shown in figure 2.11. An industry standard 1kW arcjet thruster operating on hydrogen propellant is run in a vacuum chamber located at the Electric Propulsion Laboratory of the Phillips Laboratory at Edwards Air Force Base. The arcjet operates on a hydrogen gas flow of 13.1 mg/s (8.74 slpm) at an operating chamber pressure of 6 Pa (45 mTorr). The gas flow and power are chosen to closely match the conditions under which the most complete set of previous diagnostic data for a 1 kW hydrogen arcjet is taken, in order to facilitate comparisons between different data sets and between data and models.

The laser is a pulsed dye laser pumped by a Nd:YAG with a repetition rate of 10 Hz and a pulse width of 6 ns. For the two photon direct excitation method, the dye laser output is at 615 nm and is frequency tripled using BBO crystals to achieve about 0.5 mJ per pulse at 205 nm. A mirror turns about 80% of the beam toward the arcjet chamber through a variable attenuator placed in the beam, the remaining 20% of beam energy is directed toward a microwave-discharge source of atomic hydrogen.

For the single-laser two-step technique, the dye laser output is at 486 nm and is frequency doubled using a single BBO crystal to achieve about 0.2 mJ per pulse at 243 nm (due to the weaker dye used in this wavelength range). The beams in the two-step technique need to be brought together at the detection volume both spatially and temporally so a delay line in one beam can be required.

For axial velocity measurements, the beam is sent directly down the axis of the arcjet flow (Path 1) and is focused with a telescope lens configuration (not shown) outside the chamber with a focal length on the order of 2 m. For radial measurements, the unfocused beam is sent to a turning prism inside the chamber located underneath the arcjet (Path 2), directed to pass vertically through the plume, and is focused by a 200 mm lens. The laser beam and optics remain fixed, while the arcjet is mounted on a motion control *xyz* stage to translate it for probing different regions of the plume.

A filtered PMT is placed behind the final turning mirror before the chamber in order to detect ASE that may propagate back along the laser beam path. A 200 mm focal length, 2" diameter lens is placed inside the chamber to collimate the LIF that is emitted toward the side window. The light is collected outside the chamber, focused through a 1 mm aperture, and detected with a filtered, gated PMT. Since the LIF occurs at 656 nm, the filters used are a 656 nm bandpass interference filter and an RG 645 color glass filter (thus all scattered laser light (205nm) is filtered out). The gated PMT is an ordinary Hamamatsu 928 tube with a special socket that is triggered to detect light for 2 ms during each laser pulse and is off between pulses. A gated integrator with a 30 ns gate is used to amplify and average the Hα fluorescence seen by the PMT. Alternatively, the PMT signal can be digitized by a fast oscilloscope to obtain fluorescence lifetimes and quenching information.

The weak UV beam that is sent into the discharge cell is focused with a 150 mm lens. The cell is run with a slow flow of a few Torr of helium carrier gas and a few percent hydrogen through a microwave discharge tube. The LIF is detected through a filtered (ungated) PMT. Simultaneous detection of LIF from the cell during each spectral scan of the arcjet LIF provides a zero-velocity comparison from which to measure Doppler shifts and room temperature Doppler widths. This discharge cell provides wavelength calibration but not density calibration. A separate discharge cell is used for density calibration and is placed inside the chamber when the arcjet is not operating. Density calibration is discussed in more detail below.

2.3.3.1 Calibration for absolute density measurements

The procedure for obtaining absolute number density is based on a method reported by Meier et al.[2.27-2.30] After a relative number density scan and corresponding lifetime data are taken, the arcjet is then turned off and translated away from the collection volume, the chamber is opened, and a second calibration cell is placed in the detection volume with the laser beam passing through it. The LIF signal and lifetime are measured for the hydrogen atoms present in the cell. Atoms are present due to the flow of hydrogen gas through a microwave discharge prior to entering the cell. Since the laser beam, detection optics and electronics have remained the same, the LIF from the arcjet and from the cell will have the same proportionality to absolute number density after correcting for any differences in quenching:

$$N_H^A = \frac{S^A}{S^C} \cdot N_H^C \cdot C_Q \tag{2.13}$$

Here S^A and S^C are the signal sizes (integrated over the entire spectral width) from the arcjet and the cell, N_H^A and N_H^C are the absolute number densities of atomic hydrogen in the arcjet and the cell, and C_Q is the scaling factor for the difference in quenching. C_Q is given by the ratio of fluorescence decay rate in the arcjet to that in the calibration cell.

The absolute number density of hydrogen atoms in the discharge cell is obtained using a standard chemical titration method. A schematic of the calibration cell used for this method is found in figure 2.12. The cell is made out of glass tubing and is approximately 30 cm (12 in.) long and 5 cm (2 in.) in diameter. Important to the design of the cell is the long drift tube area with a Teflon tubing liner to reduce gas/wall interactions. This drift tube allows complete mixing of the titration gas and the gas of interest. In this case, the titration gas is NO_2 and H is the gas to be calibrated.

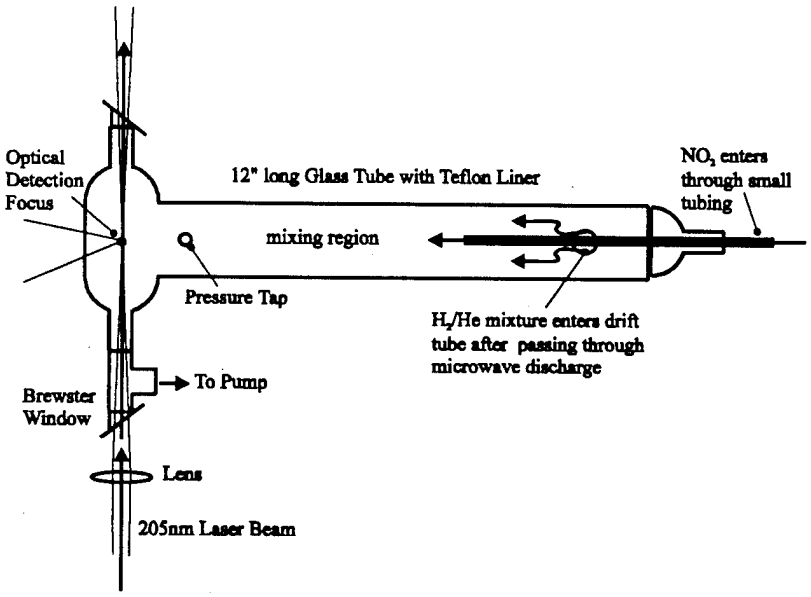

Figure 2.12. Calibration cell schematic.

The hydrogen (with a helium carrier gas) enters the drift tube area near one end after passing through a microwave discharge. A dilute mixture of NO_2 in helium is added to the flow through a long thin tube and enters the larger drift tube region at a location past the point where the hydrogen has entered. This reduces the amount of NO_2 that might diffuse upstream and enter the microwave discharge.

The NO_2 reacts rapidly with hydrogen atoms when the two are completely mixed in the large drift tube volume. The calibration involves flowing a 2% hydrogen in helium mixture and then the addition of 2% NO_2 in helium until the fluorescence signal decreases. A small vacuum pump brings the cell pressure to about a tenth of an atmosphere during this procedure.

The calibration involves observing the LIF signal decrease until it is gone at the point where the partial pressure of added NO_2 is equal to the partial pressure of hydrogen atoms in the cell. Control of the amount of NO_2 added allows the determination of the amount of hydrogen atoms present in the calibration cell. The NO_2 concentration at the point the fluorescence disappears is equal to the concentration of atomic hydrogen present as each hydrogen atom is reacted away for each NO_2 molecule added in the fast reaction

$$H + NO_2 \rightarrow OH + NO \qquad (2.14)$$

The large amount of buffer gas and low amount of H significantly reduce possible secondary reactions, making them negligible for the purposes of this experiment. Calibration takes place either before or after each arcjet firing.

Once a relative density profile has been taken as described above, and quenching, ASE, MPI, laser linewidth broadening, etc. have been compensated for or taken into account, an effective fluorescence measurement results representing relative density in the arcjet plume. Through the method described in the previous section, a relationship between H atom density and a corrected effective LIF fluorescence for the calibration cell environment may be determined. If the correction factors in each environment are appropriately made so as to bring the fluorescence measured in each environment to a standard "ideal" condition equivalent, a relationship between the fluorescence measured in the arcjet plume and the corresponding atomic hydrogen number density may be made.

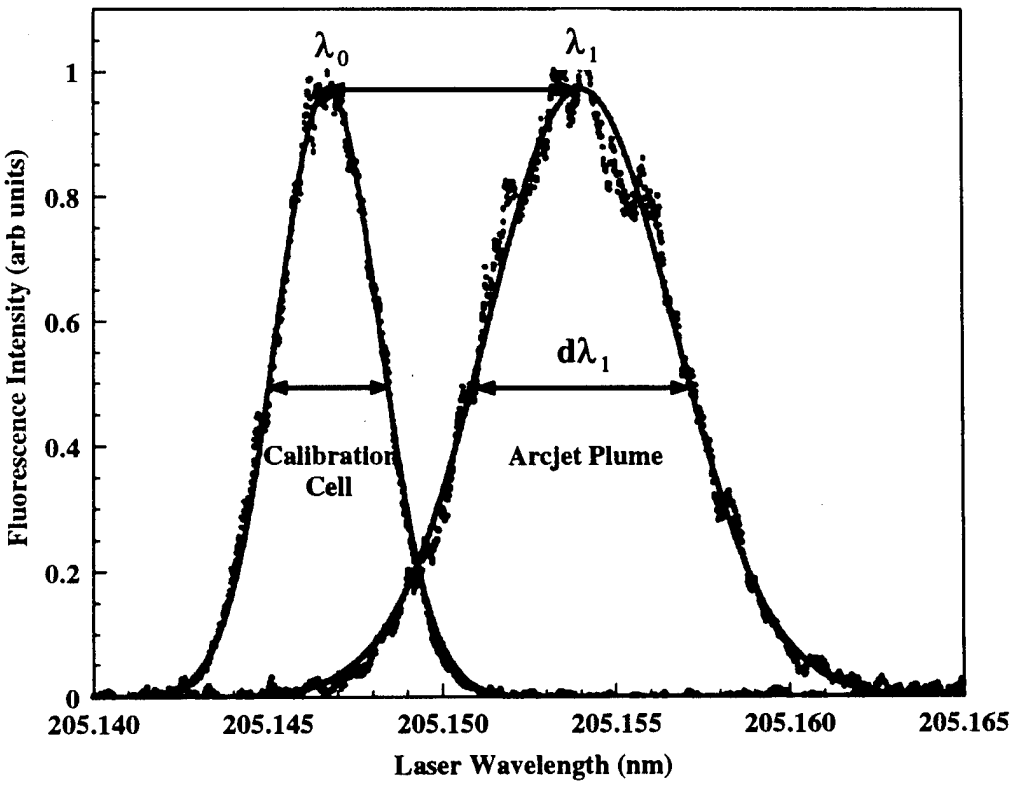

Figure 2.13. LIF spectrum of the hydrogen atom, showing the calibration signal from the discharge cell and the signal from the arcjet plume along with Gaussian least square fit profiles.

Figure 2.13 shows an axial scan involving simultaneous two-photon excitation of atomic hydrogen in a calibration cell and excitation of atomic hydrogen in a point 0.4mm away from nozzle exit in the arcjet plume. A Gaussian least-squares fit overlays the data and is used for determination of velocity, temperature, and density. Note that the fit for the cell is very good as the environment is quite static. The fit in the arcjet plume is not as good, though the fit width and center do appear to match the data quite well.

The Doppler shift of the arcjet plume absorption line relative to the static absorption in the cell is evident as is the Doppler width increase due to the much higher temperature in the arcjet plume relative to the room temperature in the calibration cell. The data correspond to a temperature near 2000K and a velocity near 10 km/s. These numbers are rough as each of the broadening mechanisms have not been fully accounted for in this analysis.

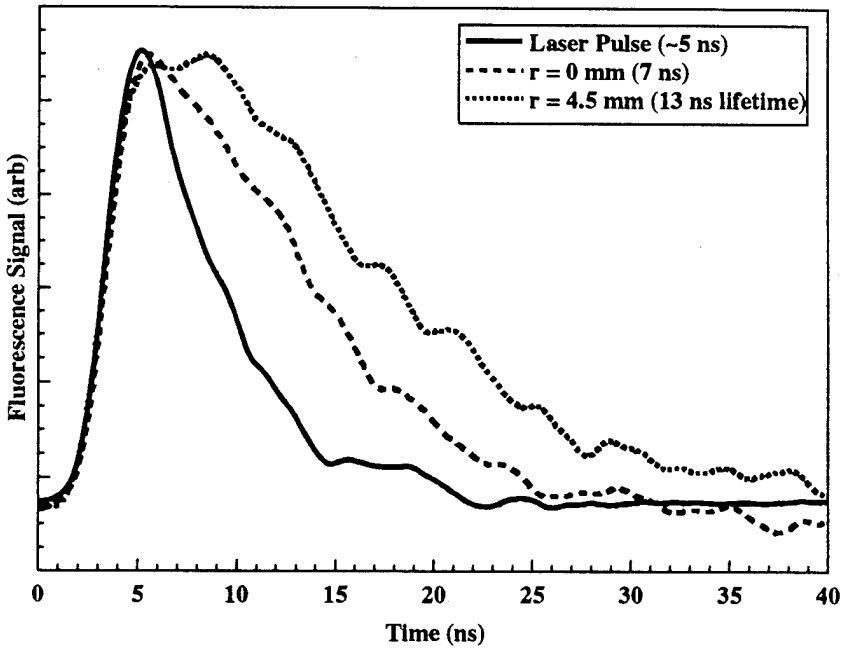

Figure 2.14. Fluorescence decay for n=3 hydrogen atoms at two positions along the arcjet nozzle exit plane. For comparison, a trace of the laser pulse alone (with no hydrogen atoms present) is shown.

To use the data in figure 2.13 for a relative density measurement the integrated area of the transition is compared with the integrated fluorescence area of data from another spatial location. To determine the correction for quenching at each spatial location, fluorescence lifetime measurements with a fast oscilloscope must be made. Figure 2.14 shows fluorescence measurements of the laser beam alone, the lifetime at the center of the plume

and the lifetime near one edge near the nozzle exit. The lifetime of the unquenched transition is 15.7ns ±1.5 ns[2.31] so some collisional quenching is still evident even near the edge of the visible plume near the nozzle exit.

2.4 Current-modulation velocimetry

Although much research, both experimental and numerical, has been conducted on arcjet plumes over the last 30 years, almost all previous studies assumed that the arcjet operates in a steady-state mode. However, when current is provided by a high frequency switching power supply, the current delivered to the arcjet is modulated at the PPU switching frequency. How current modulation affects overall arcjet thruster performance is not fully understood. Current modulation is thought to potentially play a role in electrode erosion effects, while reference [2.42] clearly demonstrated that excited state frozen flow losses are affected by current modulation. It must still be resolved how current fluctuations affect mean velocity and frozen flow: dissociation, ionization, and vibrational and rotational energy losses. Furthermore, velocity fluctuations may lead to recoverable viscous losses.

In order to obtain velocity fluctuation data in an arcjet plume, it was necessary to develop a new velocity diagnostic. This diagnostic, called current modulation velocimetry (CMV), measures instantaneous velocity over a spatial region between two points. A current spike applied to the arcjet input current generates an optical event which is observed to travel downstream with the gas flow. Observing this event at two locations a fixed distance apart implies an average bulk velocity of the gas flowing out of the arcjet nozzle. CMV is the only technique presently being employed that provides instantaneous velocity measurements of the arcjet plasma with temporal resolution of a few microseconds. The disadvantages of CMV are that it employs spatial averaging over an axial distance of several mm and that it is a line-of-sight integrated technique.

In [2.43], the CMV technique was used to measure fluctuations in velocity as large as ±20% of the mean velocity (figure 2.15). The source of the fluctuations in the gas velocity was not ascertained, though it was surmised that the velocity fluctuations might be linked to the ripple in the current applied to the arcjet.

The present work employs the use of an automated triggering circuit in conjunction with the CMV technique to measure velocity at a time when the current ripple is at a specified level. This allows multiple velocity measurements taken for statistical purposes to be triggered at the same phase in the current ripple.

CMV experiments were conducted in the Optical Diagnostics Chamber of the Air Force Phillips Laboratory Electric Propulsion Laboratory. The arcjet used here is a 1-KW-class radiatively-cooled engine, constructed and furnished by NASA Lewis Research Center. Standard operating conditions were: 1.13KW (112.5 V and 10.1 A), with 13.7 mg/s mass flow of hydrogen propellant. The experiments were conducted with a background chamber pressure of ~35 millitorr. The operating conditions are similar to those of other groups involved in optical diagnostic velocity measurements,[2.44] allowing comparison of experimental results to be made.

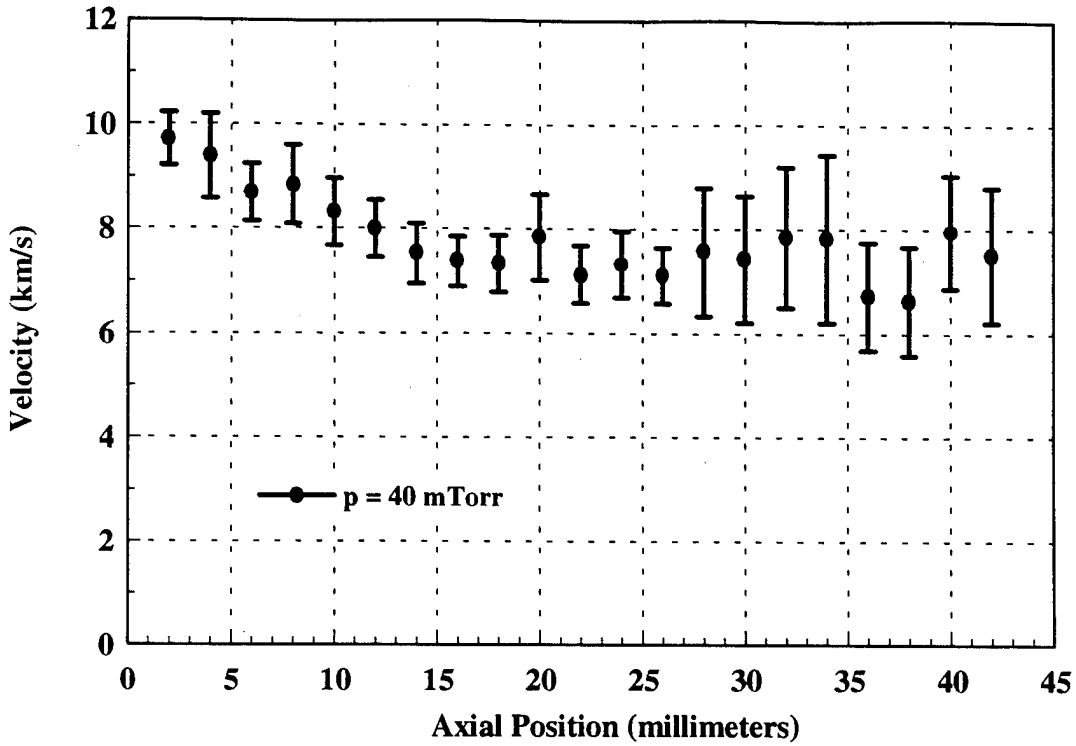

Figure 2.15. Mean velocities and fluctuations downstream of arcjet nozzle exit.

Power was provided by a NASA Lewis 1-KW power processing unit (PPU). The PPU is a high-frequency switching power supply, operating at 16 kHz, and generates a 20% peak-to-peak current ripple. The vacuum system consists of an aluminum chamber, 3 m in length and 2 m in diameter. Two 9500-cfm Roots blowers evacuate the chamber; each is backed by a 1600-cfm blower and a mechanical pump.

For the optical emission measurements, two Hamamatsu R943-02 photomultiplier tubes (PMT) were used. A 10 nm passband interference filter (Melles Griot; l_0=656.3 nm) and appropriate neutral density filters were placed in front of each PMT to insure that only the Ha emission was observed. The optics train of each detection system is identical. All optical, current and voltage signals were recorded on a Tektronix DSA 601 digital signal analyzer or a Tektronix TDS 644A digital oscilloscope.

The current spike needed for CMV is generated by a simple RC shunt circuit which is installed in parallel with the arcjet. Upon closing a switch between this circuit and the arcjet circuit, the arcjet voltage appears across the shunt, charging the capacitor over several 1-microsecond RC time constants. The shunt current is thus a several-ampere pulse lasting a few microseconds. The shunt current is subtracted from the arcjet current, which results in a spiked current dropout (the total current from the PPU is constant during this time, as it is held up by an output inductor of several mH).

The positive ring of the current pulse generates a sharp emission spike. A portion of the flow inside the arcjet is thus "tagged" by the current pulse. The emission spike is delayed with respect to the current spike; this delay is equal to the integral of $1/v$ over the distance from the arc-heating region to the detection station, where v is the plume velocity as a function of axial position.

The emission spike is recorded at two different downstream locations. A best-fit transformation between the two digitized emission spikes is determined using the standard Levenberg-Marquardt method.[2.37] The generated covariance matrix gives a measure of the confidence interval of the best-fit parameters, assuming the measurement of the optical signal to be subject to uniform, normally-distributed scatter. Error bars indicate the precision of each measured velocity and are computed using a one-standard-deviation confidence interval of the horizontal translation (the time delay between the two emission spikes).

The current and emission spikes are of a few microseconds duration. The time delay between the emission spikes at the two locations can be resolved to within one nanosecond, leading to a velocity measurement whose accuracy is in the range 30–60 m/s for plume velocities on the order 5–10 km/s; this accuracy is comparable to those of recent LIF results.[2.44–2.46]

Note that the velocity measurements obtained with CMV, while still position-averaged over the detector separation (here, 3.29±0.05 mm), are instantaneous. The principal velocity diagnostics presently being used for arcjets are continuous wave[2.44,2.45] and pulsed[2.46] LIF which provide spatially resolved mean velocity measurements but with very limited temporal resolution. LIF measurements determine the absorption lineshape by scanning in laser wavelength, which takes a minimum of several seconds to determine a velocity. In principle, a Doppler-shifted emission lineshape could be recorded instantaneously by a spectrograph and a gated imaging detector, but we know of no plume measurements in which Doppler shifts have been so measured. (In the recent Stuttgart work of Zube and Auweter-Kurtz,[2.47] instantaneous lineshapes were recorded in order to measure arc properties [gas excitation temperature and electron density].)

An automatic opto-isolated MOSFET circuit allowed computer control of the start time and duration of the modulation to the arcjet current (figure 2.16). The switch closes based upon a trigger from a pulse generator. The generator issues a pulse when the measured arcjet current reaches a pre-set level and after a computer request for an event has been received. This allows the operator to issue a request for a measurement and have that measurement take place the next time the PPU current ripple is at the specified phase.

Figure 2.17 illustrates the effect of the CMV technique on the arcjet's current and voltage. The PPU-induced arcjet current ripple is briefly interrupted while the capacitor charges. The current then rings upward and significantly overshoots its previous maximum. After quickly dampening, the current begins its previous PPU - induced ripple. Note that the voltage across the arcjet also has a characteristic ripple and that it is almost 180° out of

phase of the current. This is expected due to the negative impedance characteristic found in arcjet devices.[2.48]

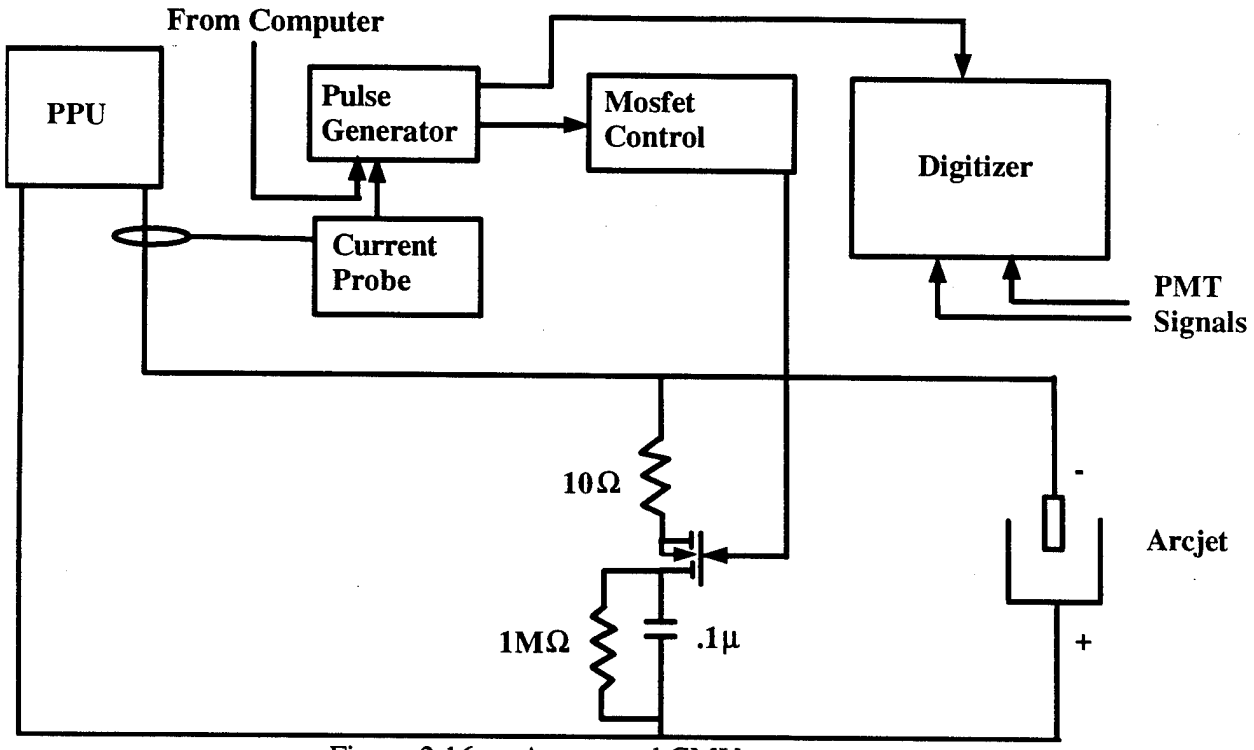

Figure 2.16. Automated CMV setup.

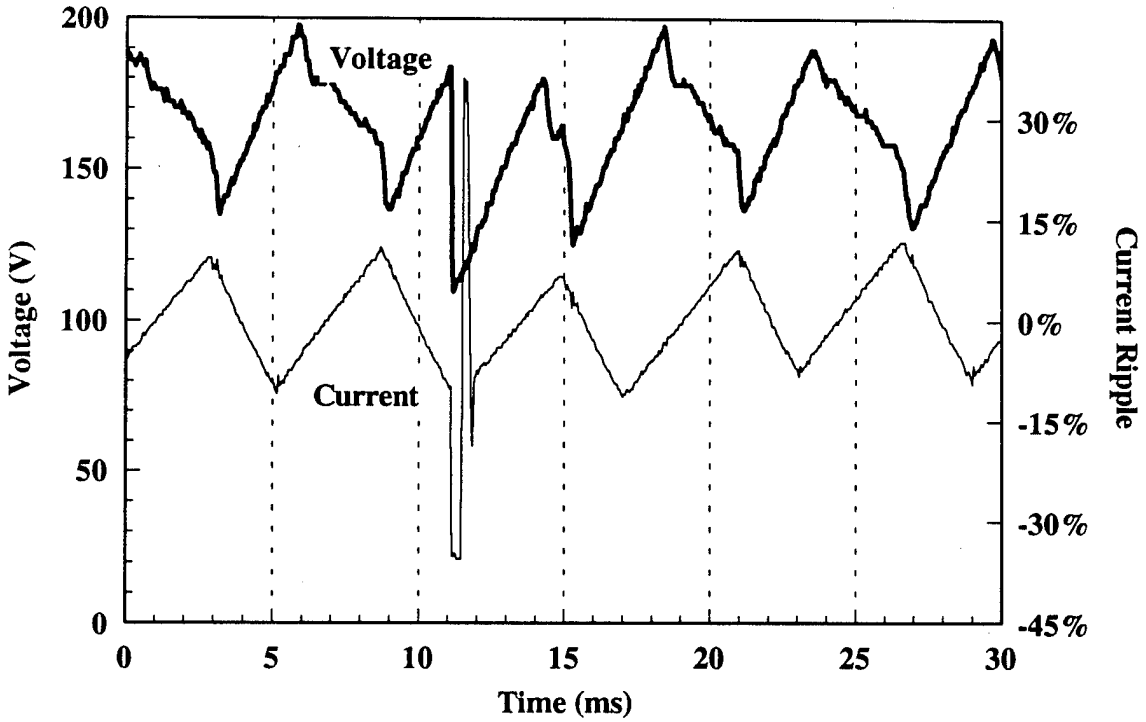

Figure 2.17. Typical CMV effect on arcjet current and voltage.

This figure reveals an unexpected behavior of the arcjet voltage which occurs as current is redirected into the capacitor of the RC circuit. The voltage drops suddenly as the current drops and then gradually ramps upward to previous levels without ringing. It then begins its periodic ripple.

Figure 2.18 gives the current and voltage on a shorter timescale. The voltage and current both drop quickly after the CMV gate pulse closes the circuit and then simultaneously change in slope. The voltage begins to ramp back upward to previous levels, while the current decreases in a more gradual way then before. At t = 11.5 microseconds, the current then shoots upward with no apparent reaction by the arcjet voltage. It then returns to previous levels with some minimal ringing.

In addition to arcjet current and voltage probes, a Hall-effect current probe was placed on the RC circuit. Two digitizing oscilloscopes were used in order to simultaneously observe several transient signals. These include the arcjet current and voltage, the current through the circuit when the switch is closed, the gate controlling the switch, and the two emission traces taken from the photomultiplier tubes. The resulting scope traces are shown together in figure 2.19.

The current measured through the circuit is complementary to the current going to the arcjet, as expected. When the circuit current drops below its initial level (no current through the circuit), it indicates that current through the circuit has reversed direction and that the capacitor is discharging; this is an expected reason for the arcjet current to overshoot. The arcjet current rapidly decreases, dropping below its initial level, and a short ring in circuit current is seen. This is followed by a slow rise back up to zero in circuit current and a return to previous ripple behavior in arc current.

As noted earlier, the arcjet voltage follows the current when the CMV gate is closed and decreases in value rapidly. As current begins to flow through the circuit, however, the arcjet voltage begins a slow rise back to its previous level, seemingly unaffected by other changes in arcjet current.

All optical events are observed downstream of the arcjet nozzle exit plane. One photomultiplier tube (with a hydrogen Balmer-alpha notch filter) is focused to a small control volume of diameter 1 mm from the nozzle exit centerline, while a second identical PMT system is focused to a control volume located 3.29 mm downstream of the nozzle exit. Noise in the optical emission, which starts at 4 msec in figure 2.19, is seen simultaneously by both PMT's when the arcjet current first begins to rise. This is then followed by a much more significant increase in Balmer-alpha emission at 6 msec. This increase occurs at both control volumes but at different times, being seen first at the upstream PMT focal point.

The optical noise seen as the arcjet current first rises does not demonstrate a time shift as does the emission that follows it. Thus, the two different emission phenomena seen at 4 and 6 msec are most likely caused by different excitation processes.

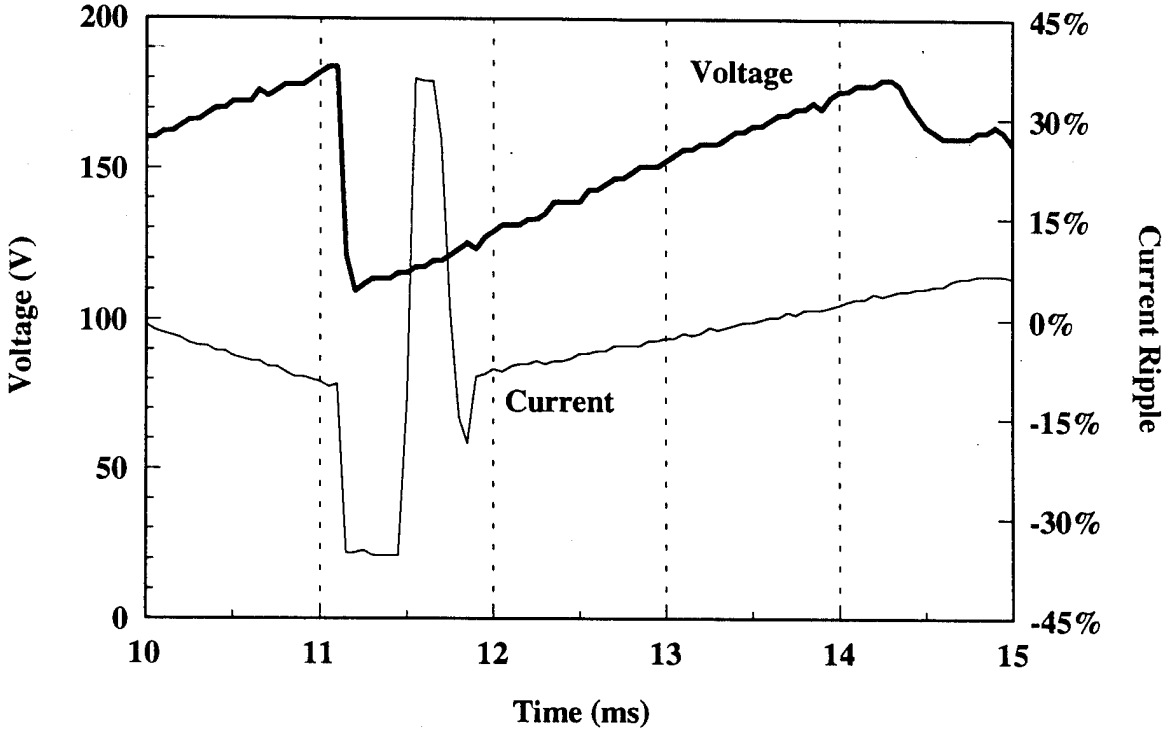

Figure 2.18. Typical CMV effect on arcjet current and voltage, shorter time scale.

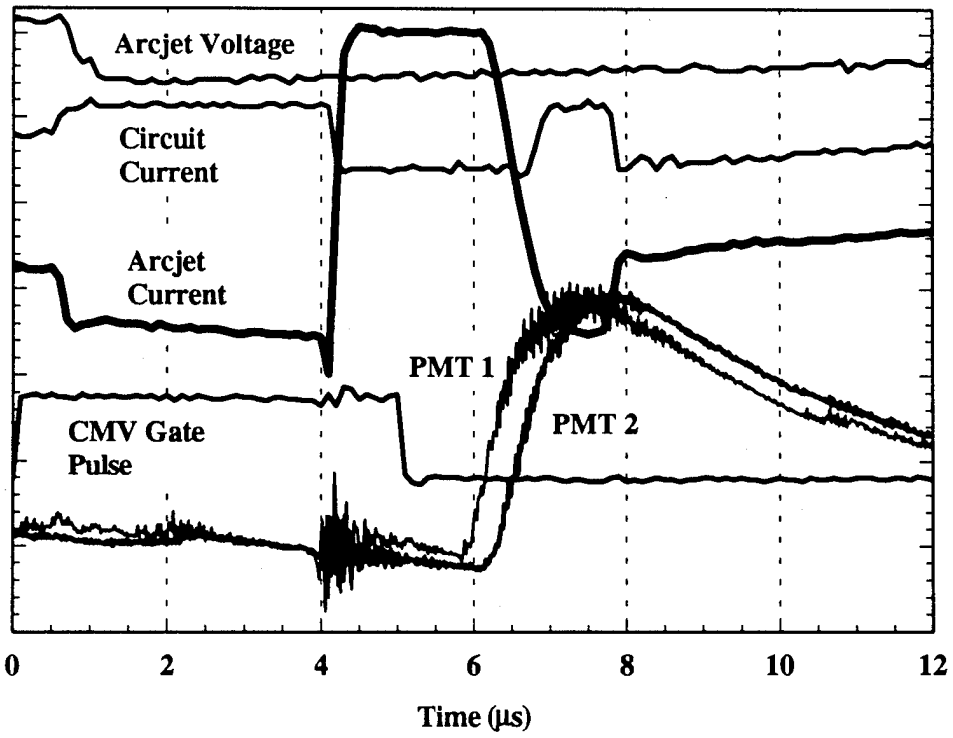

Figure 2.19. Arcjet and CMV properties vs. time (arbitrary units on vertical axis).

It was previously stated[2.43] that the optical emission phenomenon that progresses downstream in the plume comes from electron recombination which repopulates the uppermost energy levels of the H atom. The electrons subsequently cascade downward to repopulate the $n=3$ excited state which is then observed by the PMTs as Hα emission. This explanation still appears valid for the large time-dependent emission peaks which begin at 6 msec. However, the optical noise seen at 4 msec must warrant a separate explanation due to its time independent nature. It is likely that the optical emission at 4 msec in the arcjet plume is caused by the reabsorption of photons generated at the arc core inside the constrictor region of the arcjet, as suggested by Crofton et al.[2.49]

When starting the arcjet, the voltage characteristic of the thruster changes slowly as the nozzle heats up. The mean voltage increases while the heating takes place. Prior to reaching a steady-state voltage a curious behavior is noted to intermittently take place when implementing the CMV technique. Though the proper trigger gate and initial current behavior remain the same, differences in the current overshoot appear to lead to a situation where the emission spikes used for velocimetry do not appear. This situation is shown in figure 2.20.

Note that the first four microseconds of the "non-emission" case are essentially identical to the previous case depicted in figure 2.19 where Hα emission is present. The sharp rise in current that followed in the previous case is not present and both types of emission previously observed are absent. This prevents a CMV velocity measurement from being made and appears only in situations where the arcjet voltage is lower than the standard operating condition of 112.5V and 10.1A. As the arcjet is operated at lower current (and consequently higher voltage) this behavior is no longer seen. Therefore, the implementation of the CMV technique appears to rely upon a minimum voltage across the arcjet in order to generate a subsequent ringing in the arcjet current when current is redirected into an RC circuit. It is likely that this subsequent ringing is the key phenomenon, inducing the emission which proceeds downstream, and thus allowing time-of-flight velocity measurements to be made.

In order to make velocity measurements while "linked" to the PPU current ripple, a computer-controlled MOSFET gate switch was implemented. In using this switch a new parameter in CMV operation was required, this being the length of time that the RC circuit was closed (the gate width) in parallel with the arcjet. Results from varying the gate width are shown in figure 2.21.

The gate width was varied from ½ ms to 100's of ms in length. The mean velocity measured was basically the same as long as the gate width was above 3 ms. Mean velocities measured were observed to decrease as the pulse width was decreased for the equivalent test conditions. Figure 2.21 demonstrates this behavior for three different power conditions. The $\frac{P}{\dot{m}}$ was held constant by reducing the mass flow through the

arcjet as power was decreased. Note that for the 1.13KW case, the decrease in velocity measured was less evident than in the lower power cases.

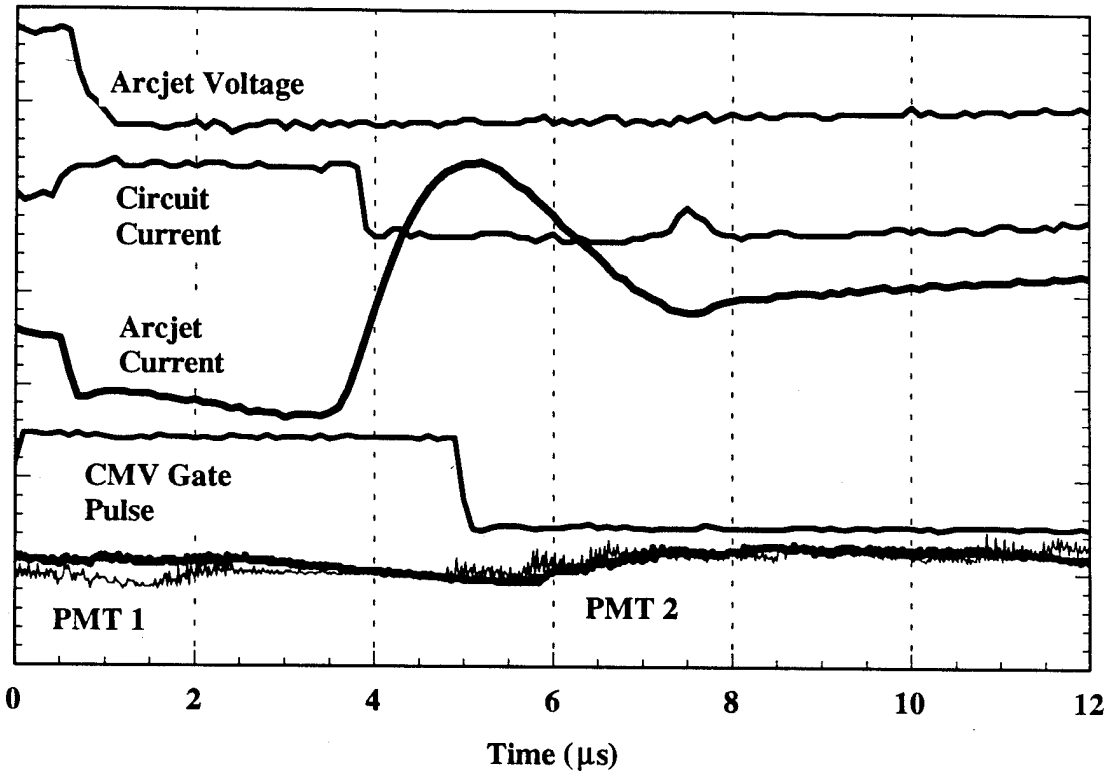

Figure 2.20. Arcjet and CMV properties vs. time: no CMV emission.

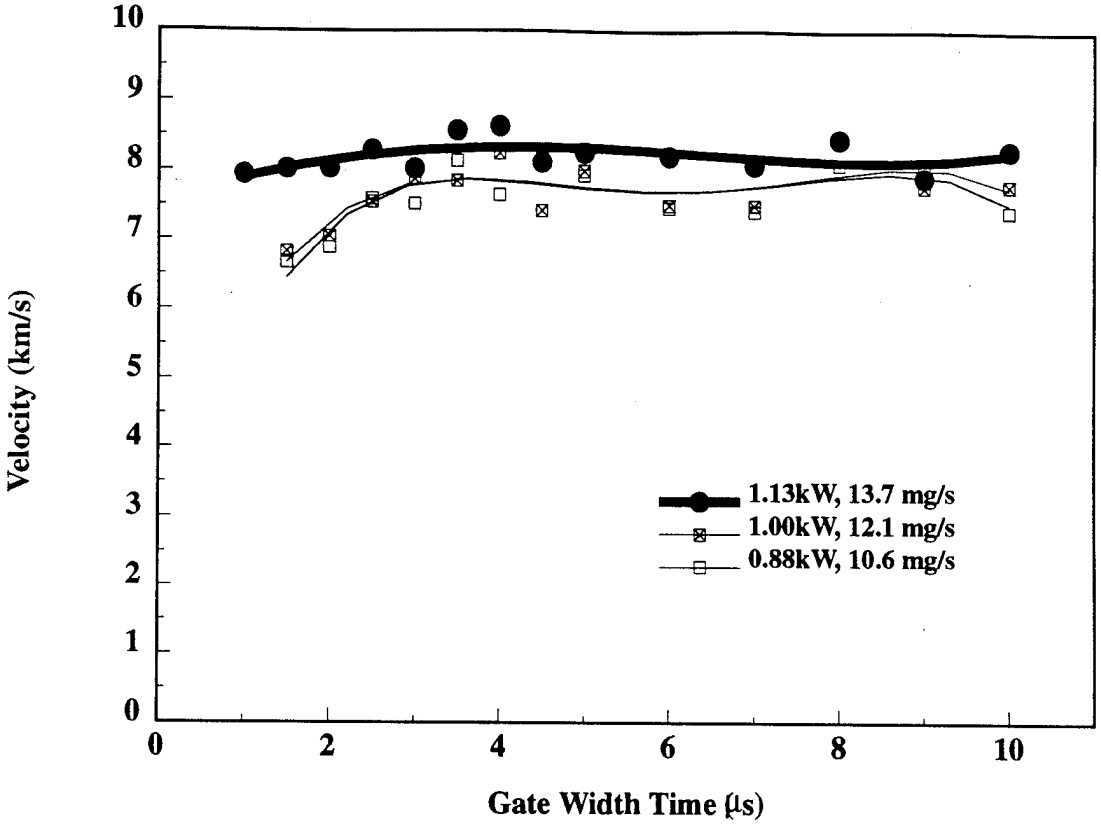

The shorter gate widths cause a change in "measured" velocity between the two emission collection points in the plume. When the RC circuit is connected to the arcjet for less than 3 microseconds, the behavior of current and voltage is similar to that seen in Figure 7 where the voltage is insufficient for CMV emission to take place. The short-gate-width behavior differs from that of figure 2.20 since CMV emission occurs, though at lower intensities than desirable.

These lower velocity measurements are not due to a lower signal intensity but are suspect in the fact that the emission shape is less defined. It is possible that the recombination processes that repopulate the uppermost electronic levels are incomplete when the circuit is in parallel with the arcjet for short durations. We surmise that the lower velocities result from utilizing a waveform that undergoes change as it traverses between the two imaging control volumes.

The average velocity measured at the nozzle exit, as well as the standard deviation of velocity fluctuations using CMV with a gate width larger than 3 microseconds, is shown in figure 2.22 along with LIF longitudinal velocity data from Liebeskind et al.[2.50]

In this figure, radial, point-specific, time-averaged LIF velocity measurements are compared with a line-of-sight-averaged CMV velocity shown as a line across the graph, with two dashed lines representing the standard deviation of observed velocity fluctuations. Though the density of excited-state H is not available to weigh the LIF data and obtain an mean LIF velocity, relatively good agreement between these two techniques is observed.

It has previously been surmised that the fluctuations shown in Figure 9 and in our previous work[2,43] have been a consequence of the oscillating nature of the internal energy dissipation of a 1KW arcjet due to the PPU current modulations. Triggering at a constant PPU ripple level, figure 2.23 shows measured mean velocity and standard deviations while triggering at constant current ripple phase.

In figure 2.23, no change in mean velocity value or substantive change in fluctuations can be directly related to PPU phase angle. If the velocity is changing with respect to the current ripple, a significant decrease in fluctuation and change in mean velocity should be observed.

With no apparent connection between the PPU ripple and the mean velocity, the question arises once again: What is causing the fluctuations in arcjet plume velocity? Attempts at determining a fluctuation frequency through a real-time transformation of the difference between the emission from the two imaging points provide inconclusive results. Certainly finding a fundamental frequency of velocity fluctuation might narrow the possible causes of this phenomenon, though it remains to be seen if a single cause can be pinpointed.

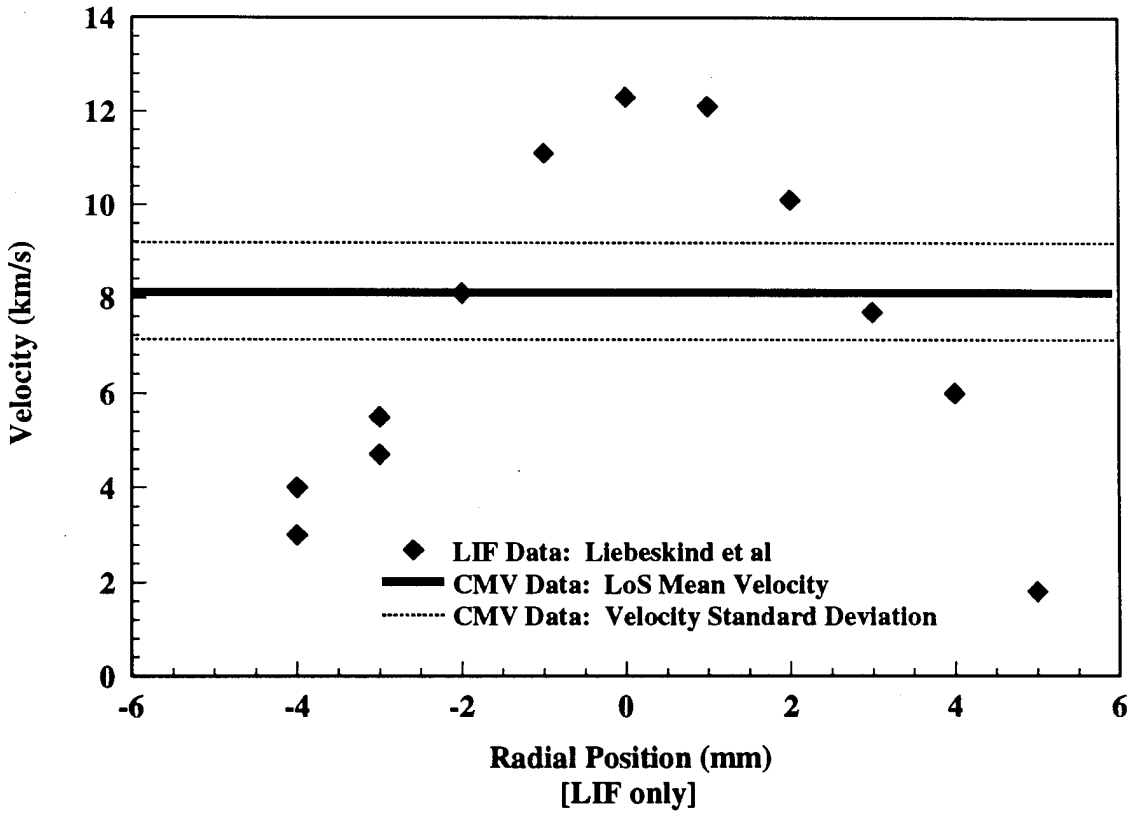

Figure 2.22. CMV and LIF 1kW arcjet velocities at nozzle exit.

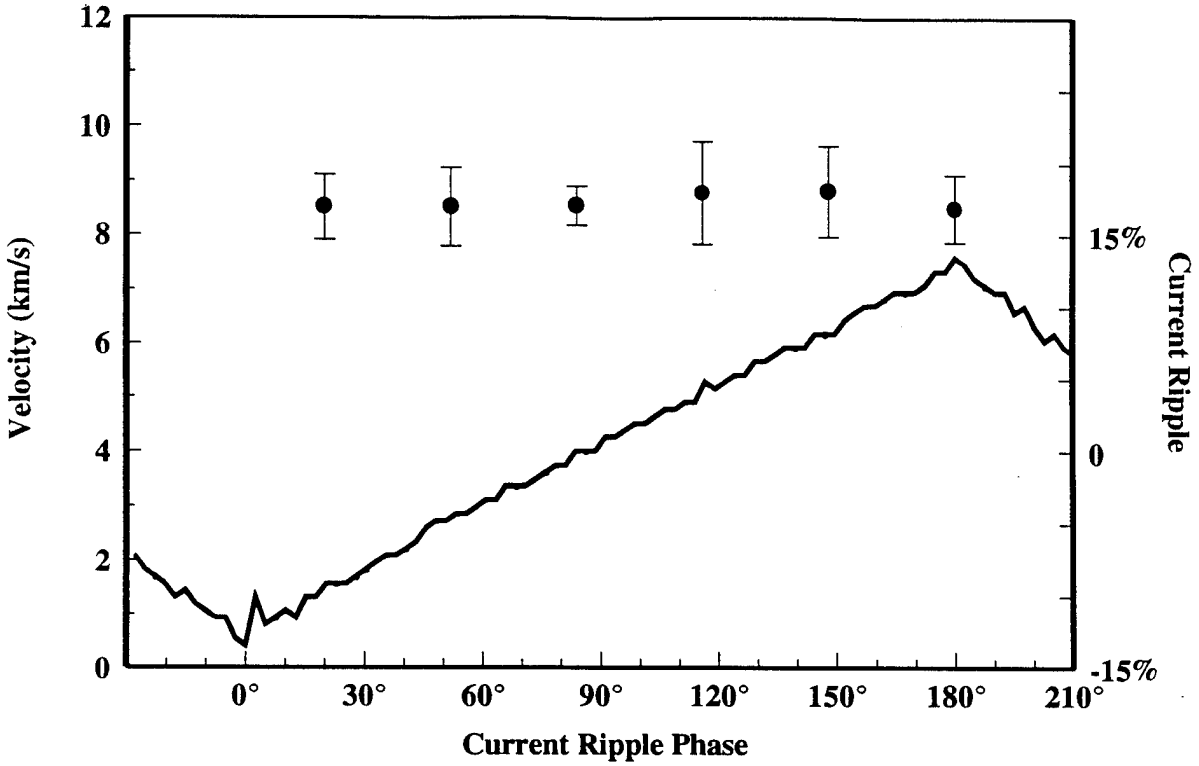

Figure 2.23. CMV exit plane velocity measurements at various current ripple phases.

3. Conclusions

In this work, several innovative approaches to experimental diagnostics of arcjet operation have been developed. For the first time, measurements of ground state atomic hydrogen have been made in a powered-up arcjet. These measurements are in accord with published computational results to within the experimental accuracy. These measurements need to be extended to produce a comprehensive density map of the plume; this part of the work was expected to be completed during the period of the contract, but both density-measurement techniques (pulsed electron-beam fluorescence and two-photon laser-induced fluorescence) experienced unexpected protraction during development and are only now reaching sufficient maturity.

The other technique used in this work, current-modulation velocimetry, has been applied to the problem of measuring the time dependence of arcjet plume velocity fluctuations. These fluctuations turn out to bear no measurable correlation with supply current ripple, and appear to be random. The impact of this conclusion on time-dependent arcjet modeling is not yet obvious.

References

1.1. W. W. Smith, IEPC-91-148, 1991.

1.2. C. E. Vaughan and R. J. Cassady, AIAA- 92-3202, 1992.

1.3. D. A. Erwin, G. C. Pham-Van-Diep, and W. D. Deininger, AIAA Journal **29**, 1298 (1991).

1.4. J. G. Liebeskind, R. K. Hanson, and M. A. Cappelli, Appl. Opt. **32**, 6117 (1993).

1.5. D. H. Manzella and M. A. Cappelli, AIAA-92-3564, 1992.

1.6. J.E. Pollard, AIAA-92-2966, 1992.

1.7. D. Keefer, D. Burtner, T. Moeller, and R. Rhodes, AIAA-94-2656, 1994.

1.8. G. W. Butler, I. D. Boyd, and M. A. Cappelli, AIAA-95-2819, 1995.

1.9. V. Babu, S. M. Aithal, and V. V. Subramaniam, AIAA-94-2655, 1994.

1.10. S. Miller and M. Martinez-Sanchez, IEPC-93-218, 1993.

1.11. T. W. Megli, H. Krier, R. L. Burton, and A. E. Mertogul, AIAA-94-2413, 1994.

1.12. I. D. Boyd, M. A. Cappelli, and D. R. Beattie, AIAA-93-2529, 1993.

1.13. D. R. Beattie and M. A. Cappelli, AIAA-92-3566, 1992.

1.14. D. R. Beattie and M. A. Cappelli, AIAA-95-1956, 1995.

2.1. E. P. Muntz, AGARDograph 132, 1968.

2.2. K. A. Buetefisch and D. Vennemann, Prog. Aerosp. Sci. **15**, 217 (1974).

2.3. J. A. Smith and J. F. Driscoll, J. Fluid Mech. **72**, 695 (1975).

2.4. H. Alsmeyer, J. Fluid Mech. **72**, 695 (1975).

2.5. E. P. Muntz, "Measurement of density by analysis of electron beam excited radiation," in *Methods of Experimental Physics*, R. J. Emrich, ed. (Academic, New York, 1981).

2.6. E. P. Muntz, "Measurement of temperature by analysis of electron beam excited radiation," in *Methods of Experimental Physics*, R. J. Emrich, ed. (Academic, New York, 1981).

2.7. D. J. McCaa and D. E. Rothe, Symposium on Molecular Structure and Spectroscopy, 1968.

2.8. T. Holstein, Phys. Rev. **72**, 1212 (1947).

2.9. T. Holstein, Phys. Rev. **83**, 1159 (1951).

2.10. J. H. Lees and H. W. B. Skinner, Proc. Roy. Soc. **A137**, 186 (1932).

2.11. R. M. St. John, A. A. Bronco, and R. G. Fowler, J. Opt. Soc. Am. **50**, 28 (1960).

2.12. C. C. Lin and R. M. St. John, Phys. Rev. **128**, 1749 (1962).

2.13. E. P. Muntz, Phys. of Fluids **11**, 64 (1968).

2.14. D. E. Rothe, Phys. of Fluids **9**, 1643 (1966).

2.15. R. E. Center, Phys. of Fluids **10**, 1777 (1968).

2.16. K. Frank and J. Christiansen, IEEE Trans. Plasma Sci. **17**, 748 (1989).

2.17. W. Benker, J. Christiansen, K. Frank, H. Gundel, W. Hartmann, T. Redel, and M. Stetter, IEEE Trans. Plasma Sci. **17**, 754 (1989).

2.18. J. E. M. Goldsmith, J. A. Miller, R. J. M. Anderson, and L. R. Williams, Proc. 23rd Int'l Symposium on Combustion, 1821 (1990).

2.19. J. E. M. Goldsmith and L. A. Rahn, Opt. Lett. **15**, 814 (1990).

2.20. J. E. M. Goldsmith and N. M. Laurendeau, Opt. Lett. **15**, 576 (1990).

2.21. J. E. M. Goldsmith, Appl. Opt. **15**, 4841 (1990).

2.22. J. E. M. Goldsmith, R. J. M. Anderson, and L. R. Williams, Opt. Lett. **15**, 78 (1990).

2.23. U. Westblom, S. Agrup, M. Alden, H. M. Hertz, and J. E. M. Goldsmith, Appl. Phys. B **50**, 487 (1990).

2.24. J. E. M. Goldsmith, J. Opt. Soc. Am. B **6**, 1979 (1989).

2.25. J. E. M. Goldsmith, Proc. 22nd Int'l Symposium on Combustion, 1403 (1988).

2.26. J. E. M. Goldsmith, Opt. Lett. **10**, 116 (1985).

2.27. U. Meier, K. Kohse-Hoinghaus, L. Schaefer, and C.-P. Klages, Appl. Opt. **29**, 4993 (1990).

2.28. J. Bittner, K. Kohse-Hoinghaus, U. Meier, S. Kelm, and T. H. Just, Combustion and Flame **71**, 41 (1988).

2.29. U. Meier, J. Bittner, K. Kohse-Hoinghaus, and T. H. Just, Proc. 22nd Int'l Symposium on Combustion, 1887 (1988).

2.30. U. Meier, K. Kohse-Hoinghaus, and T. H. Just, Chem. Phys. Lett. **126**, 567 (1986).

2.31. A. D. Tserepi, J. R. Dunlop, B. L. Preppernau, and T. A. Miller, J. Appl. Phys. **72**, 2638 (1992).

2.32. B. L. Preppernau, D. A. Dolson, R. A. Gottscho, and T. A. Miller, Plasma Chem. and Plasma Proc. **9**, 157 (1989).

2.33. U. Czarnetski, K. Miyazaki, T. Kajiwara, K. Muraoka, M. Maeda, and H. F. Dobele, J. Opt. Soc. Am. B **11**, 2155 (1994).

2.34. K. Muraoka and M. Maeda, Plasma Phys. Controlled Fusion **35**, 633 (1993).

2.35. A. C. Eckbreth, *Laser Diagnostics for Combustion Temperature and Species*, 1st ed. Kent: Abacus, 1988.

2.36. W. Demtröder, *Laser Spectroscopy: Basic Concepts and Instrumentation.* Berlin: Springer, 1988.

2.37. W. H. Press, B. P. Flannery, S. A. Teukolsky, and W. T. Vetterling, *Numerical Recipes: The Art of Scientific Computing*, 1st ed. Cambridge: Cambridge, 1986.

2.38. D. J. Bamford, L. E. Jusinski, and W. K. Bischel, Phys. Rev. **A 34**, 185 (1986).

2.39. N. Georgiev, K. Nyholm, R. Fritzon, and M. Alden, Opt. Comm. **108**, 71 (1994).

2.40. M. S. Brown and J. B. Jeffries, Appl. Opt. **34**, 1127 (1995).

2.41. P. V. Storm and M. A. Cappelli, AIAA-95-1960, 1995.

2.42. R. A. Spores, J. A. Pobst, J. H. Schilling, and D. A. Erwin, AIAA-92-3238, 1992.

2.43. J. A. Pobst, J. H. Schilling, D. A. Erwin, and R. A. Spores, IEPC-93-128, 1993.

2.44. J. G. Liebeskind, R. K. Hanson, and M. A. Cappelli, AIAA-93-2530, 1993.

2.45. W. M. Ruyten and D. Keefer, IEPC-91-093, 1991.

2.46. D. A. Erwin, G. C. Pham-Van-Diep, and W. D. Deininger, AIAA Journal **29**, 1298 (1991).

2.47. D. M. Zube and M. Auweter-Kurtz, AIAA-93-1792, 1993.

2.48. E. J. Pencil, J. M. Sankovic, C. J. Sarmiento, and J. A. Hamley, AIAA-92-3530, 1992.

2.49. M. W. Crofton, R. P. Welle, S. W. Janson, and R. B. Cohen, AIAA-91-1491, 1991.

2.50. M. A. Cappelli, J. G. Liebeskind, R. K. Hanson, G. W. Butler, and D. Q. King, IEPC-93-220, 1993.